Lung interstitial macrophages can present soluble antigens and induce Foxp3⁺ regulatory T cells

Authors

Céline Legrand[1], Domien Vanneste[2,3], Alexandre Hego[4], Catherine Sabatel[1,2], Kiréna Mollers[1], Joey Schyns[1,2], Pauline Maréchal[2,3], Joan Abinet[3], Amandine Tytgat[1], Maude Liégeois[1], Barbara Polese[1], Margot Meunier[2,3], Coraline Radermecker[2,3], Laurence Fiévez[1,2], Fabrice Bureau[1,2,*] & Thomas Marichal[2,3,5,*].

Affiliations

[1] Laboratory of Cellular and Molecular Immunology, GIGA Institute, Liège University, Liège, Belgium

[2] Faculty of Veterinary Medicine, Liège University, Liège, Belgium

[3] Laboratory of Immunophysiology, GIGA Institute, Liège University, Liège, Belgium

[4] In Vitro Imaging Platform, GIGA Institute, Liège University, Liège, Belgium.

[5] Walloon Excellence in Life Sciences and Biotechnology (WELBIO) Department, WEL Research Institute, Wavre, Belgium

[*] These authors contributed equally to this work and are co-last authors

Author contributions

FB and TM conceived, supervised and secured funding for the project. CL, FB and TM designed the experiments. CL did most of the experiments with the help of CS, KM, JS, PM, JA, AT, ML, BP, MM, CR and LF. CL compiled the data and prepared the figures. DV did the scRNAseq data analyses. AH performed the spatial distribution analysis on confocal microscopy pictures. TM wrote the manuscript with the help of CL. All authors provided feedback on the manuscript.

Correspondence

Fabrice Bureau

Laboratory of Cellular and Molecular Immunology,

GIGA Institute, Liege University,

Quartier Hôpital, B34,

Avenue de l'Hôpital 11,

4000 Liege, Belgium

f.bureau@uliege.be

Thomas Marichal

Laboratory of Immunophysiology,

GIGA Institute, Liege University,

Quartier Hôpital, B34,

Avenue de l'Hôpital 11,

4000 Liege, Belgium

t.marichal@uliege.be

Abstract

Lung macrophages constitute a sophisticated surveillance and defense system that contributes to tissue homeostasis, host defense, and allows the host to cope with the myriad of insults and antigens to which the lung mucosa is exposed. As opposed to alveolar macrophages, lung interstitial macrophages (IMs) express high levels of type 2 major histocompatibility complex (MHC-II), a hallmark of antigen-presenting cells. Here, we showed that lung IMs, like dendritic cells (DCs), possess the machinery to present soluble antigens in an MHC-II-restricted way. Using *ex vivo* ovalbumin (OVA)-specific T cell proliferation assays, we found that OVA-pulsed IMs could trigger OVA-specific $CD4^+$ T cell proliferation and Foxp3 expression via MHC-II-, IL-10- and Tgfβ-dependent mechanisms. Moreover, we showed that IMs efficiently captured locally instilled antigens *in vivo*, did not migrate to the draining lymph nodes and enhanced local interactions with $CD4^+$ T cells in a model of OVA-induced allergic asthma. These results support that IMs can present antigens to $CD4^+$ T cells and trigger regulatory T cells, which might attenuate lung immune responses and have functional consequences for lung immunity and T-cell-mediated disorders.

Introduction

Mammalian lungs are at the interface between the host and the external world and are continuously exposed to pathogens, allergens, microbial products and other insults. In order to allow efficient gas diffusion and to support life, the airways must be permeable and the air-blood barrier must remain very thin. Accordingly, the lung innate immune system has evolved as a sophisticated surveillance and defense system to sustain physiological functions and host protection while avoiding deleterious immunopathological responses (1–5). Distinct lung myeloid cell populations are dedicated to these tasks in the lung, including resident tissue macrophages (RTM), tissue monocytes (Mo) and dendritic cells (DCs)(4, 6–10).

The well-known alveolar macrophages (AMs) are self-maintaining RTM specialized in removal of cell debris, recycling of surfactant and represent the first responders to lung insults (4, 11, 12). AMs do not express MHC-II at steady-state (10, 13, 14). The lung also contains a network of Irf8-dependent type 1 DCs (cDC1s) and Irf4-dependent type 2 DCs (cDC2s), which are considered as professional antigen-presenting cells that initiate $CD8^+$ T cell and $CD4^+$ T helper (Th) cell responses in the draining lymph nodes, respectively, thereby bridging lung innate and adaptive immunity (9, 15–17). Like DCs, lung $Ly6C^+$ tissue Mo express MHC-II and can sample and transport antigens to the draining lymph nodes (8).

The diversity and biology of lung interstitial macrophages (IMs) is arguably more complex, as IMs are present in relatively low numbers at steady-state and populate the parenchyma, rendering them less accessible than AMs. In adults, IMs are slowly replenished by $Ly6C^+$ classical Mo (13, 14, 18, 19), require the transcription factor MafB for their differentiation (19) and encompass distinct subsets based on their phenotype and on their localization around the bronchi, the nerves or the blood vessels (13, 18–22). Briefly, we and others have reported the existence of $CD11c^{lo}Lyve1^{hi}CD206^+$ IMs and $CD11c^{int/hi}Lyve1^{lo}CD206^-$ IMs, called $CD206^+$ IMs and $CD206^-$

IMs hereafter, respectively. CD206$^+$ IMs express low levels of MHC-II, represent a major source of the immunoregulatory cytokine interleukin(IL)-10 and preferentially associate with blood vessels and the bronchi, consistent with blood vessel-supportive and immunosuppressive functions (13, 14, 18, 20). Besides CD206$^+$ IMs, CD206$^-$ IMs express high levels of MHC-II, are located in the vicinity of nerve bundles and their homeostatic functions remain, to date, unknown (13, 18, 20). Ural and colleagues independently reported the existence of a nerve-associated IM subset, called NAM, expressing CD169 and preferentially located around the airways (21). The phenotypical similarities between NAM and CD206$^-$ IMs support that both subsets overlap, at least partially. Functionally, NAM were found to attenuate influenza virus-triggered pathology (21). More recently, a population of CD11c$^+$Cx3cr1^{hi}MHC-II^{hi} bronchus-associated macrophages, called BAM, was reported to be capable of antigen presentation and local Th2 activation (22), supporting the novel idea that the ability to present antigens and trigger Th2 allergic responses is not merely restricted to DCs, as previously thought (15, 16, 23).

Even though IMs represent a heterogenous population and a consensus still needs to be found about the precise localization of IM subsets within their niches, the existence of IMs expressing CD11c and MHC-II, like DCs, is well accepted (10, 13, 14, 18, 20, 22). Here, we sought to evaluate the ability of steady-state IMs to capture soluble antigens and present them to naive CD4$^+$ T cells. We found that IMs captured intratracheally-administered ovalbumin (OVA) and presented OVA-derived epitopes in an MHC-II-restricted way. IMs were able to trigger the proliferation of OVA-specific CD4$^+$ T cells *ex vivo* as efficiently as DCs. Such T cells acquired a Foxp3$^+$ regulatory phenotype in an IL-10- and Tgfβ-dependent manner, consistent with IM immunoregulatory properties. Lastly, we revealed enhanced interactions between IMs and CD4$^+$ T cells in a mouse model of OVA-induced allergic asthma *in vivo*, suggesting a local contribution of IMs to the regulation of lung CD4$^+$ T cell responses.

Methods

Mice

C57BL/6J WT mice were purchased from Charles River. *Il10*$^{-/-}$ (B6.129P2-*Il10*^{tm1Cgn}/J), OTII (B6.Cg Tg(TcraTcrb)425Cbn/J) and *Cx3cr1*$^{GFP/GFP}$ (B6.129P-Cx3cr1tm1Litt/J) mice under the C57BL/6J background were purchased from the Jackson Laboratory (Cat. #002251, 004194, and 005582, respectively).

All mice were housed and bred in institutional SPF facilities at the GIGA Institute (Liège University, Belgium), maintained in a 12-h light-dark cycle, and had access to normal diet chow and water *ad libitum*. Male and female mice were used at 7–11 weeks of age. Additional details can be found in the data supplement.

Reagent and antibodies

Ovalbumin and LPS were from Sigma (reference A5503 and L4524, respectively). OVA-FITC was from Davids biotechnologies (reference 16-0003-01). See Table E1 for the complete references of antibodies used in this study.

Antigen instillation and experimental asthma induction *in vivo*

For antigen administration *in vivo*, lightly isoflurane-anesthetized mice were administrated with 100 or 25 µg OVA, 100 or 125 µg OVA-FITC and eventually 1 µg LPS (Sigma) in 50 µL intratracheally (i.t.).

For experimental asthma induction, lightly isoflurane-anesthetized *Cx3cr1*$^{GFP/+}$ mice were sensitized by two weekly i.t. instillations of PBS (Gibco) or OVA (100 µg in 50 µL) at days 0 and 7. Mice were then challenged by four i.t. instillations of PBS or OVA (25 µg in 50 µL) at days 16 to 19 and were sacrificed at day 20.

129

130 **scRNA-seq analyses**

131 Methods related to scRNA-seq analyses can be found in the data supplement.

132

133 **Cell Isolation, Staining and Flow cytometry**

134 Briefly, to obtain single-lung-cell suspensions, lungs were enzymatically digested as described
135 previously (13, 14). The suspension was then filtered and enriched in mononuclear cells by using
136 a density gradient (phenotyping) or enriched by MACS using anti-mouse CD11b microbeads
137 (sorting). Lymph nodes were digested in 1mL of the same digestion medium for 15 min at 37°C.
138 Staining reactions were performed at 4 °C. Additional details can be found in the data supplement.

139

140 **APC-L_T coculture experiments**

141 Lung IMs and $CD11b^+$ cDCs were FACS-sorted from $CD11b^+$ cell-enriched lung single cell
142 suspensions of C57BL/6 WT or *Il10*$^{-/-}$mice, while AMs were FACS-sorted from the $CD11b^-$
143 fraction of WT mice. Naïve T lymphocytes were obtained by crushing lymph nodes and spleens
144 of OT-II mice using a flat-bottomed syringe in 1 mL of PBS-EDTA. Cells were stained with the
145 naïve CD4+ T cell isolation kit (Miltenyi Biotec) according to manufacturer instructions and were
146 separated on LS columns (Miltenyi Biotec) on a QuadroMacs (Miltenyi Biotec). For proliferation
147 assays, enriched T cells were washed with PBS, and labeled with Cell Tracer Yellow (CTY -
148 Invitrogen), as described(24). Cells were cultured in 96 round-bottomed wells plates in RPMI with
149 L-Glutamine (Lonza) completed with 10 % FBS (Gibco), 50 U/mL penicillin/streptomycin
150 (Gibco), 1 % MEM non-essential amino acids (Gibco), 1 mM sodium pyruvate (GE Healthcare)
151 and 0.05 mM 2-mercaptoethanol (Gibco) at a ratio of 1 cDC, IM or AM for 2 L_T for 3 days. For
152 Foxp3 induction assays, lung AMs, cDCs and IMs were seeded with OVA and the naive T

lymphocytes were added the next day. We analyzed the Foxp3 expression using the Foxp3/Transcription factor staining buffer set (Invitrogen) 5 days later.

In some experiments, OVA (125 µg/mL), MHC-II Ab or control isotypes (20µg/mL), Tgfβ Ab or control isotype (1 µg/mL), IL-10 Ab or control isotype (1 µg/mL) or rTGFβ1 (1ng/mL) were added in the co-culture. See Supplementary Table 1 for detailed references.

Confocal microscopy stainings

Methods related to confocal microscopy stainings can be found in the data supplement.

Confocal microscopy acquisition and analysis

Methods related to confocal microscopy acquisition and analysis can be found in the data supplement.

Statistical analyses

Data from independent experiments were pooled for analysis in each data panel, unless otherwise indicated. Statistical analyses were performed using Prism 7 (GraphPad Software). Data were presented as mean ± S.D., as well as individual values, unless otherwise indicated. We considered a P value lower than 0.05 as significant. *, $P < 0.05$; **, $P < 0.01$, ***, $P < 0.001$; ****, $P < 0.0001$; ns, not significant. Details about the statistical tests used can be found in the respective Figure legends.

Results

Lung IMs express high levels of MHC-II and genes related to the MHC-II machinery

We evaluated the expression of MHC-II on lung AMs, IMs, Mo and cDCs subsets from wild-type C57BL/6 mice by flow cytometry using previously published gating strategies (9, 14). We identified $CD45^+SSC^{hi}F4/80^+CD11c^+$ AMs, $CD45^+SSC^{lo}CD11b^+F4/80^+Ly6C^-CD64^+$ IMs, $CD45^+SSC^{lo}CD11b^+F4/80^+Ly6C^+CD64^-$ classical Mo (cMo), $CD45^+SSC^{lo}CD11b^+F4/80^+Ly6C^-CD64^-$ patrolling Mo (pMo), $CD45^+Lin^-CD11c^+MHC\text{-}II^+CD64^-CD26^+CD172a^-$ cDC1s, $CD45^+Lin^-CD11c^+MHC\text{-}II^+CD64^-CD26^+CD172a^+$ cDC2s and monocyte-derived $CD64^+$ cells (MCs), defined as $CD45^+Lin^-CD11c^+MHC\text{-}II^+CD64^+CD26^-CD172a^+$ cells (9), which encompassed CD11c-expressing IMs (Figure E1). Confirming previous reports (10, 13, 14, 18, 20, 22), we found that IMs, like cDC1s and cDC2s, expressed high levels of MHC-II, unlike AM (Figures 1A and 1B), consistent with the idea that IMs can present epitopes in a MHC-II-restricted way.

To further address the antigen-presenting potential of IMs, we assessed the expression of genes involved in the MHC-II processing machinery, namely genes coding for the H-2 class II histocompatibility antigen (*H2-Ab1*), the chaperone molecule γ chain of MHC-II (*Cd74*), the CLIP exchanger H2-DMb1 (*H2-DMb1*) and MHC-II degradative cathepsin enzymes (*Ctsh, Ctsc*). To this end, we interrogated two published sets of scRNA-sequencing data from IMs (9, 13) and cDCs (9) subsets. The uniform manifold approximation and projection (UMAP) plots and cell clusters are shown in Figure 1C. To formally assess whether MCs indeed encompassed IMs in the dataset of Bosteels et al. (9), we mapped a IM signature score on their datasets, and showed that cluster 7 (C7), corresponding to MCs, exhibited the highest IM score, and was therefore named

198 "MC-IMs" (Figure 1D). Interestingly, both CD206$^-$ IMs and CD206$^+$ IMs (13) expressed
199 significantly higher levels of *H2-Ab1, Cd74, H2-DMb1, Ctsh* and *Ctsc* compared to CD16.2$^+$
200 monocytes and AMs (Figure 1E). Moreover, we found that MC-IMs (C7) expressed similar or
201 higher levels of *H2-Ab1, Cd74, H2-DMb1, Ctsh* and *Ctsc* compared to all the lung cDC subsets
202 (Figure 1F). Altogether, these results support that IMs possess the required machinery to present
203 antigens via the MHC-II machinery.
204
205 **Lung IMs can trigger proliferation of antigen-specific CD4$^+$ T cells via MHC-II *ex vivo***
206 Next, we aimed to assess whether lung primary IMs could trigger the proliferation of antigen-
207 specific naïve CD4$^+$ T cells *ex vivo*. To this end, IMs and CD11b$^+$ cDCs were FACS-sorted from
208 CD11b$^+$ cell-enriched lung single cell suspensions of C57BL/6 mice, while AMs were FACS-sorted
209 from the CD11b$^-$ fraction (Figure E2, A-E). Sorted cells were cocultured for 3 days with Cell
210 Tracer Yellow (CTY)-labeled naïve CD4$^+$ T lymphocytes (L_T) (Figure E2F) from ovalbumin
211 (OVA)-specific, MHC-II-restricted, TCR transgenic OT-II C57BL/6 mice in the presence or
212 absence of OVA (Figure 2A). An average of 83, 88 and 25 % of proliferating L_T were detected in
213 the presence of IMs, CD11b$^+$ cDCs and AMs, respectively (Figures 2B and 2C), suggesting that
214 IMs are as potent as CD11b$^+$ cDCs in activating naive L_T, while AMs are poor inducers of L_T
215 proliferation. No proliferation was observed in the absence of OVA (Figures 2D and 2E), nor in
216 the presence of anti-MHC-II antibodies (MHC-II Ab) (Figures 2F and 2G), demonstrating that
217 IM- and CD11b$^+$ cDC-mediated L_T proliferation was antigen-specific and MHC-II-dependent.
218 The ability of IMs to trigger T cell proliferation was significantly higher for MHC-II^{hi} IMs than
219 for MHC-II^{lo} IMs, even though both IM subsets were able to present OVA (Figures 2H and 2I).
220
221 **IMs can induce Foxp3$^+$ regulatory CD4$^+$ T cells via IL-10- and Tgfβ-dependent mechanisms**

IMs constitutively produce IL-10 and can exert important immunoregulatory functions in the context of experimental asthma (10, 14, 25). In light of these considerations, we wondered whether IMs could preferentially induce regulatory T cells (T_{reg}) as compared to CD11b$^+$ cDCs. Hence, we employed the same coculture system as described above and evaluated the numbers of Foxp3$^+$ L_T after 5 days of coculture (Figure 3A). Of note, the number of Foxp3$^+$ L_T was significantly higher in the IM:L_T coculture as compared to the CD11b$^+$ cDC:L_T coculture and to the AM:L_T coculture (Figures 3B and 3C).

Next, we interrogated the scRNA-seq data of lung myeloid cells presented in Figure 1 for expression of transcripts involved in T_{reg} induction (26–29). Of note, many of the transcripts were little expressed, except *Tgfb1* detected in every myeloid cell population (Figure 3D and Figure E3). *Aldh1a2*, coding for retinaldehyde dehydrogenase, was expressed at a significantly higher level in migratory cDC1s as compared to each other clusters (Figure E3C), as expected (28). *Il10* transcript levels were very low, but were nevertheless higher in a fraction of both IM subsets as compared to AMs, monocytes and cDCs (Figure 3D and Figure E3), consistent with the known ability of IMs to constitutively produce IL-10 at steady-state (10, 13, 14). Given the important roles of IL-10 and Tgfβ in the induction and maintenance of induced T_{reg} (30–32), we aimed to evaluate the contribution of these immunosuppressive cytokines in IM-mediated T_{reg} induction. First, we found that the numbers of Foxp3$^+$ L_T were significantly lower in IM:L_T cocultures in the presence of anti-Tgfβ Ab (Figures 3E and 3F). Second, we observed a significant decrease in numbers of Foxp3$^+$ L_T in IM:L_T cocultures in the presence of anti-IL-10 Ab (Figures 3G and 3H). Third, to address the contribution of IM-intrinsic IL-10 in T_{reg} induction, we compared IM:L_T cocultures with IM isolated from wild-type (WT) or from *Il10*$^{-/-}$ mice and found that the numbers of Foxp3$^+$ L_T were significantly lower when IM were not able to produce IL-10 (Figures 3I and 3J). Finally, we found that addition of recombinant Tgfβ (rTgfβ) in the coculture potentiated the ability of

IM to induce T_{reg} (Figures 3K and 3L), while it had no effect on CD11b$^+$ cDC-mediated T_{reg} induction (Figure E4). Altogether, these results support that lung IMs can induce Foxp3$^+$ L_T *ex vivo* via IM-intrinsic IL-10-dependent mechanisms, and that Tgfβ contributes to the expansion of T_{reg}.

Efficient capture of OVA by IMs *in vivo* allows antigen-specific T cell proliferation and Foxp3$^+$ regulatory T cell induction *ex vivo*

So far, IMs were pulsed with OVA *ex vivo*, and it remains to be determined whether efficient antigen capture by IMs also occurs *in vivo* after local instillation of OVA. To test this, we exposed WT mice to FITC-labeled OVA (OVA-FITC) intratracheally (i.t.) and assessed uptake of OVA-FITC by IMs, AMs, cDC1s and cDC2s at different time point post-injection by flow cytometry, using the gating strategy shown in Figure E1. We found that IMs, cDC1s, cDC2s and AMs were able to efficiently uptake OVA-FITC, as early as 30 minutes post-injection, as shown by the high percentage of FITC$^+$ cells in every cell population (Figures 4A and 4B). In order to verify that OVA-FITC uptake occurred *in vivo* and not during the process of tissue digestion after sacrifice, we mixed lung pieces isolated from OVA-FITC-exposed CD45.2$^+$ mice with lung pieces isolated from unexposed CD45.1$^+$ mice and co-digested and co-processed them together (Figure E5A). We found that the vast majority of FITC$^+$ cDCs, IMs and AMs originated from CD45.2$^+$ mice, not from CD45.1$^+$ mice, demonstrating that the uptake of OVA-FITC indeed happened *in vivo*, and not during sample processing post-mortem (Figure E5B).

Next, we wondered whether antigen uptake *in vivo* was followed by antigen presentation and was sufficient to trigger T cell proliferation and T_{reg} induction *ex vivo.* First, we exposed WT mice to OVA in the presence of lipopolysaccharide (LPS) i.t., and FACS-sorted CD11b$^+$ cDCs, IMs and AMs 3 hours later before coculturing them with OVA-specific, CTY-labeled L_T in the

absence of OVA in the coculture (Figure 4C). After 3 days, we evaluated the percentage of proliferating L_T by flow cytometry and found that IMs and CD11b$^+$ cDCs from OVA-exposed mice, but not from PBS-exposed mice, were able to trigger L_T proliferation *ex vivo* (Figures 4D and 4E), demonstrating that *in vivo* OVA uptake is associated with efficient antigen presentation and L_T proliferation. Second, we assessed whether IMs isolated from OVA-administered mice could induce T_{reg} *ex vivo*. We employed the same coculture system as above and evaluated the numbers of Foxp3$^+$ L_T after 5 days of coculture (Figure 4F). We found that IMs could trigger OVA-specific Foxp3$^+$ L_T, which was not the case for AMs (Figures 4G and 4H). Third, as cDC1s were likely excluded by the sorting protocol used to isolate CD11b$^+$ cDCs, we assessed the ability of cDC1s and cDC2s sorted from OVA-administered mice to trigger Foxp3$^+$ L_T in the same coculture system and found a tendency of cDC1s to induce more Foxp3$^+$ L_T than cDC2s, even though it did not reach statistical significance (Figure E6), in line with previous findings (28).

Evidence of enhanced local IM-L_T interactions in a model of OVA-induced asthma

Finally, we wondered whether IMs could interact with L_T *in vivo*, and where this interaction would take place. First, we assessed the migratory abilities of IMs as compared to cDC1s and cDC2s by assessing the numbers of FITC$^+$ cells present in the lung draining lymph node 20 hours after i.t. exposure to OVA-FITC and LPS (Figure 5A and Figure E7). While FITC$^+$ cDC1s and cDC2s were recruited to the lymph nodes, no evidence of FITC$^+$ IMs was found (Figures 5B and 5C), suggesting that IMs did not migrate, as suggested previously (22). Second, we performed immunostainings of CD4$^+$ T cells and *Cx3cr1*^{GFP}/MHC-II$^+$ IMs (13, 18) on lung sections from wild-type mice that were chronically exposed to OVA (as a model of experimental asthma) or exposed to PBS as vehicle (Figure 5D). Of note, CD4$^+$ L_T were found in the vicinity of IMs in control and asthmatic lungs (Figure 5E). We evaluated the intercellular distance between CD4$^+$ L_T

294 and IMs and found that IM distance to the nearest $CD4^+$ L_T was significantly decreased in
295 asthmatic mice, with a substantial increase in IM-$CD4^+$ L_T pairs that were distant from less than
296 10 μm (Figures 5F and 5G). These data suggest that IM-L_T interactions occur *in vivo* and are
297 enhanced during experimental asthma *in vivo*.
298

Discussion

Here, we found that an important functional feature of lung IMs, as opposed to the well-known AMs, was their ability to take up and present soluble antigens to L_T and endow them with a $Foxp3^+$ regulatory phenotype. We showed that Tgfβ and IM-intrinsic IL-10 contributed to this process and found evidence of enhanced IM-$CD4^+$ L_T interactions in an allergic asthma model, raising the possibility that IMs can control adaptive T cell responses in the lung.

Initial studies investigating IM functions in rodents focused on their putative interactions with DCs (10, 33) and on their ability to inhibit their function and prevent DC-mediated type 2 allergic immune responses via IL-10-dependent mechanisms (10). The current work extends our knowledge about the immunoregulatory properties of IMs by providing evidence that they can also interact with $CD4^+$ L_T and act as antigen-presenting cells by triggering antigen-specific T_{reg} via MHC-II-dependent mechanisms. Hence, there seems to be a division of labor between DCs, which can migrate to the draining LN and prime adaptive T cell responses (9, 15–17), and IMs, which might act as local regulators of adaptive T cell responses in the lung, as it has been suggested for DCs and macrophages in the intestinal mucosa (27, 34–36).

While the antigen-presenting ability of macrophages is known for decades (37, 38), few reports have specifically looked at the antigen-presenting capabilities of lung IMs (13, 18, 22). In 2013, an elegant report from Soroosh and colleagues provided experimental evidence that lung-resident tissue macrophages could generate T_{regs} and suppress allergic inflammation when adoptively transferred into asthmatic mice (39), consistent with our findings. Hoffmann and colleagues also found that IMs were more efficient as DCs in taking up antigens (40). More recently, we (13) and others (18) have characterized $CD206^+Lyve1^{hi}$ IMs and $CD206^-Lyve1^{lo}$ IMs and have shown that the $CD206^-$ IM subset possessed features of antigen-presenting cells and higher antigen presentation abilities as compared $CD206^+$ IMs. Recently, Tang *et al.* recently

investigated the localization, antigen capture, antigen presentation and behavior of a subset of bronchus-associated CD11c^{+}Cx3cr1^{hi}MHC-II^{hi} IMs, called BAMs (22). While we did not specifically investigated BAMs in our study, we showed that IMs could capture airway-instilled antigens, had poor migratory abilities, could interact with T cells locally, and were able to trigger L_T proliferation *ex vivo,* all functional features that are shared between BAMs and IMs. These data are consistent with the idea that BAMs represent indeed a subpopulation of IMs. Here, we showed that FACS-sorted IMs could promote expansion of Foxp3^{+} T_{regs}, and that Tgfβ and IM-intrinsic IL-10 contributed to this process. Interestingly, the addition of recombinant Tgfβ boosted the ability of IMs to expand T_{regs} but did not have any effect on the ability of cDCs to trigger T_{regs}, supporting that the combination of Tgfβ with another IM-derived signal, perhaps IL-10, are required to promote T_{reg} expansion, consistent with the important roles of these cytokines in tolerance induction (29). In the report of Tang *et al.*, the authors did not assess the ability of BAMs to trigger T_{regs}, but rather found that BAMs were as efficient as DCs in inducing the type 2 cytokine IL-13 from OVA-specific L_T *ex vivo* (22). Whether this relates to different microbial exposures in distinct animal facilities, or a different sorting strategy of BAMs (22) *vs.* bulk IMs, or additional factors, remains an open question.

The objective of our work was to evaluate the antigen presentation potential of IMs at steady-state. When homeostasis is broken and inflammation develops, additional monocytes are recruited to tissues and differentiate into inflammatory monocyte-derived macrophages that can overlap phenotypically with IMs and can also express high levels of MHC-II (4, 13, 14). As transgenic tools allowing the distinction between steady-state IMs and recruited macrophages are currently lacking, future work will be needed to discriminate between the ability of these recruited monocyte-derived macrophages *vs.* of *bona fide* steady-state IMs to produce IL-10 upon instillation of OVA and LPS and to influence local T cell responses via MHC-II *in vivo*. In addition, our data

347 are mainly based on *ex vivo* assays and do not prove that presentation of soluble antigens and T_{reg}
348 induction by IMs occurs *in vivo* and is relevant in the context of lung immunity and the
349 attenuation of allergic asthma or other T-cell-mediated diseases. To fully address this interesting
350 question, a novel mouse strain in which IMs, but not DCs nor monocytes, would be conditionally
351 deficient in MHC-II, would be needed.

352 As a conclusion, we showed that steady-state lung IMs possess all the necessary machinery
353 to take up, process and present soluble antigens to L_T. They can trigger their proliferation and
354 differentiation into T_{regs} *ex vivo* via IL-10 and Tfgβ-dependent pathways. Our data therefore
355 suggest that IM immunoregulatory properties might be mediated by a direct effect on the
356 differentiation of T_{regs} *in vivo*, at least in part.

357

Acknowledgements

We thank all members of the Immunophysiology and Cellular and Molecular Immunology laboratories (GIGA Institute, Liège, Belgium) for discussions; Laurence Fievez, Christophe Desmet and Catherine Sabatel for their precious help and advices; Sandra Ormenese, Raafat Stefan, Gaetan Lefevre and Céline Vanwinge from the GIGA In Vitro Imaging Platform; Pierre Drion, Gaëlle Lambert, Margaux Merchie, Benoît Remy and all staff members from the GIGA Mouse facility and Transgenics Platform; and Cédric François, Raja Fares, Ilham Sbai and Axelle Lio for their excellent technical and administrative support.

Thomas Marichal acknowledges support from the F.R.S-FNRS (Incentive Grant for Scientific Research), from the FRFS-Welbio and from the Acteria Foundation. Thomas Marichal is supported by a Research Project Grant of the F.R.S.-FNRS, by a FRFS-Welbio Advanced Grant (WELBIO-CR-2022A-10), by an ERC Starting Grant (ERC StG 2018 IM-ID: 801823), by the Baillet Latour Fund, by an 'Action de Recherche Concertée de la Fédération Wallonie-Bruxelles de Belgique' and by the Léon Fredericq Foundation. Fabrice Bureau acknowledges support from the FRFS-Welbio and is supported by an Excellence of Science (EOS) program from the F.R.S.-FNRS and FWO.

References

1. Staub NC. Pulmonary intravascular macrophages. *Annu Rev Physiol* 1994;56:47–67.
2. Martin TR, Frevert CW. Innate Immunity in the Lungs. *Proc Am Thorac Soc* 2005;2:403–411.
3. Bals R, Hiemstra PS. Innate immunity in the lung: how epithelial cells fight against respiratory pathogens. *Eur Respir J* 2004;23:327–333.
4. Aegerter H, Lambrecht BN, Jakubzick CV. Biology of lung macrophages in health and disease. *Immunity* 2022;55:1564–1580.
5. Ardain A, Marakalala MJ, Leslie A. Tissue-resident innate immunity in the lung. *Immunology* 2020;159:245–256.
6. Lambrecht BN, Hammad H. The airway epithelium in asthma. *Nat Med* 2012;18:684–92.
7. Schyns J, Bureau F, Marichal T. Lung Interstitial Macrophages: Past, Present, and Future. *J Immunol Res* 2018;2018:5160794.
8. Jakubzick C, Gautier EL, Gibbings SL, Sojka DK, Schlitzer A, Johnson TE, *et al.* Minimal differentiation of classical monocytes as they survey steady-state tissues and transport antigen to lymph nodes. *Immunity* 2013;39:599–610.
9. Bosteels C, Neyt K, Vanheerswynghels M, van Helden MJ, Sichien D, Debeuf N, *et al.* Inflammatory Type 2 cDCs Acquire Features of cDC1s and Macrophages to Orchestrate Immunity to Respiratory Virus Infection. *Immunity* 2020;52:1039-1056.e9.
10. Bedoret D, Wallemacq H, Marichal T, Desmet C, Quesada Calvo F, Henry E, *et al.* Lung interstitial macrophages alter dendritic cell functions to prevent airway allergy in mice. *J Clin Invest* 2009;119:3723–38.

11. Schneider C, Nobs SP, Kurrer M, Rehrauer H, Thiele C, Kopf M. Induction of the nuclear receptor PPAR-gamma by the cytokine GM-CSF is critical for the differentiation of fetal monocytes into alveolar macrophages. *Nat Immunol* 2014;15:1026–37.
12. Guilliams M, De Kleer I, Henri S, Post S, Vanhoutte L, De Prijck S, *et al.* Alveolar macrophages develop from fetal monocytes that differentiate into long-lived cells in the first week of life via GM-CSF. *J Exp Med* 2013;210:1977–92.
13. Schyns J, Bai Q, Ruscitti C, Radermecker C, De Schepper S, Chakarov S, *et al.* Non-classical tissue monocytes and two functionally distinct populations of interstitial macrophages populate the mouse lung. *Nat Commun* 2019;10:3964.
14. Sabatel C, Radermecker C, Fievez L, Paulissen G, Chakarov S, Fernandes C, *et al.* Exposure to Bacterial CpG DNA Protects from Airway Allergic Inflammation by Expanding Regulatory Lung Interstitial Macrophages. *Immunity* 2017;46:457–473.
15. Lambrecht BN, De Veerman M, Coyle AJ, Gutierrez-Ramos JC, Thielemans K, Pauwels RA. Myeloid dendritic cells induce Th2 responses to inhaled antigen, leading to eosinophilic airway inflammation. *J Clin Invest* 2000;106:551–9.
16. Plantinga M, Guilliams M, Vanheerswynghels M, Deswarte K, Branco-Madeira F, Toussaint W, *et al.* Conventional and monocyte-derived CD11b(+) dendritic cells initiate and maintain T helper 2 cell-mediated immunity to house dust mite allergen. *Immunity* 2013;38:322–335.
17. Schuijs MJ, Hammad H, Lambrecht BN. Professional and "Amateur" Antigen-Presenting Cells In Type 2 Immunity. *Trends Immunol* 2019;40:22–34.
18. Chakarov S, Lim HY, Tan L, Lim SY, See P, Lum J, *et al.* Two distinct interstitial macrophage populations coexist across tissues in specific subtissular niches. *Science* 2019;363:.

19. Vanneste D, Bai Q, Hasan S, Peng W, Pirottin D, Schyns J, *et al.* MafB-restricted local monocyte proliferation precedes lung interstitial macrophage differentiation. *Nat Immunol* 2023;24(5):827-840.

20. Gibbings SL, Thomas SM, Atif SM, McCubbrey AL, Desch AN, Danhorn T, *et al.* Three Unique Interstitial Macrophages in the Murine Lung at Steady State. *Am J Respir Cell Mol Biol* 2017;57:66–76.

21. Ural BB, Yeung ST, Damani-Yokota P, Devlin JC, de Vries M, Vera-Licona P, *et al.* Identification of a nerve-associated, lung-resident interstitial macrophage subset with distinct localization and immunoregulatory properties. *Sci Immunol* 2020;5(45):eaax8756.

22. Tang X-Z, Kreuk LSM, Cho C, Metzger RJ, Allen CDC. Bronchus-associated macrophages efficiently capture and present soluble inhaled antigens and are capable of local Th2 cell activation. *Elife* 2022;11:e63296.

23. Lambrecht BN, Hammad H. The immunology of asthma. *Nat Immunol* 2015;16:45–56.

24. Quah BJC, Warren HS, Parish CR. Monitoring lymphocyte proliferation in vitro and in vivo with the intracellular fluorescent dye carboxyfluorescein diacetate succinimidyl ester. *Nat Protoc* 2007;2:2049–2056.

25. Kawano H, Kayama H, Nakama T, Hashimoto T, Umemoto E, Takeda K. IL-10-producing lung interstitial macrophages prevent neutrophilic asthma. *Int Immunol* 2016; 28(10):498-501.

26. Baban B, Chandler PR, Sharma MD, Pihkala J, Koni PA, Munn DH, *et al.* IDO activates regulatory T cells and blocks their conversion into Th17-like T cells. *J Immunol* 2009;183:2475–2483.

27. Murai M, Turovskaya O, Kim G, Madan R, Karp CL, Cheroutre H, *et al.* Interleukin 10 acts on regulatory T cells to maintain expression of the transcription factor Foxp3 and suppressive function in mice with colitis. *Nat Immunol* 2009;10:1178–1184.

28. Khare A, Krishnamoorthy N, Oriss TB, Fei M, Ray P, Ray A. Cutting edge: inhaled antigen upregulates retinaldehyde dehydrogenase in lung CD103+ but not plasmacytoid dendritic cells to induce Foxp3 de novo in CD4+ T cells and promote airway tolerance. *J Immunol* 2013;191:25–29.

29. Li MO, Flavell RA. Contextual regulation of inflammation: a duet by transforming growth factor-beta and interleukin-10. *Immunity* 2008;28:468–476.

30. Groux H, O'Garra A, Bigler M, Rouleau M, Antonenko S, de Vries JE, *et al.* A CD4+ T-cell subset inhibits antigen-specific T-cell responses and prevents colitis. *Nature* 1997;389:737–742.

31. Chen Y, Kuchroo VK, Inobe J, Hafler DA, Weiner HL. Regulatory T cell clones induced by oral tolerance: suppression of autoimmune encephalomyelitis. *Science* 1994;265:1237–1240.

32. Schmitt EG, Williams CB. Generation and function of induced regulatory T cells. *Front Immunol* 2013;4:152.

33. Gong JL, McCarthy KM, Rogers RA, Schneeberger EE. Interstitial lung macrophages interact with dendritic cells to present antigenic peptides derived from particulate antigens to T cells. *Immunology* 1994;81:343–351.

34. Hadis U, Wahl B, Schulz O, Hardtke-Wolenski M, Schippers A, Wagner N, *et al.* Intestinal tolerance requires gut homing and expansion of FoxP3+ regulatory T cells in the lamina propria. *Immunity* 2011;34:237–246.

35. Farache J, Zigmond E, Shakhar G, Jung S. Contributions of dendritic cells and macrophages to intestinal homeostasis and immune defense. *Immunol Cell Biol* 2013;91:232–239.

36. Denning TL, Wang Y, Patel SR, Williams IR, Pulendran B. Lamina propria macrophages and dendritic cells differentially induce regulatory and interleukin 17-producing T cell responses. *Nat Immunol* 2007;8:1086–1094.

37. Unanue ER. Antigen-presenting function of the macrophage. *Annu Rev Immunol* 1984;2:395–428.

38. Underhill DM, Bassetti M, Rudensky A, Aderem A. Dynamic interactions of macrophages with T cells during antigen presentation. *J Exp Med* 1999;190:1909–1914.

39. Soroosh P, Doherty TA, Duan W, Mehta AK, Choi H, Adams YF, *et al.* Lung-resident tissue macrophages generate Foxp3+ regulatory T cells and promote airway tolerance. *J Exp Med* 2013;210:775–788.

40. Hoffmann FM, Berger JL, Lingel I, Laumonnier Y, Lewkowich IP, Schmudde I, *et al.* Distribution and Interaction of Murine Pulmonary Phagocytes in the Naive and Allergic Lung. *Front Immunol* 2018;9:1046.

Figure legends

Figure 1. Lung IMs express MHC-II and MHC-II processing-related genes. (A) Representative flow cytometry histograms of MHC-II (H2-Ab1) expression (red) and control isotypes (blue) in lung AMs, IMs, classical monocytes (cMo), patrolling monocytes (pMo), cDC1s, cDC2s and monocyte-derived CD64+ cells (MCs). (B) Quantification of MHC-II geometric mean in the lung myeloid cells analyzed in A, normalized to isotype. (C) UMAP plots of the scRNA-seq data analyzed from E-MTAB-7678 (13) (left) and from GSE149619 (9) (right). (D) IM signature score in lung cDC subtypes analyzed in Bosteels et al. (9). (E) Expression of the indicated genes in lung CD16.2^{+} monocytes, CD206^{+} IMs, CD206^{-} IMs and AMs, as depicted by violin plots (height: expression level; width: abundance of cells). (F) Expression of the indicated genes in lung cDC subsets, plasmacytoid DCs (pDCs) and MC-IMs, as depicted by violin plots (height: expression level; width: abundance of cells). (B) Data show the mean +/- SD and are pooled from two independent experiments, each symbol representing individual mice (n=7). *P* values were calculated with a non-parametric Kruskal-Wallis test with multiple comparisons. (E-F) To compare C2 – CD206^{-}IMs, C3 – CD206^{+} IMs (E) and C7 – MC-IMs (F) with other groups, *P* values were calculated using a Wilcoxon rank sum test. *, $P < 0.05$; **, $P < 0.01$; ***, $P < 0.001$; ****, $P<0.0001$; ns, not significant.

Figure 2. IMs can trigger proliferation of OVA-specific L_T in a MHC-II-restricted manner. (A) Experimental outline. Primary IMs, CD11b$^+$ cDCs or AMs were cocultured with CTY-labeled OVA-specific naïve L_T for 3 days, and L_T proliferation was assessed by flow cytometry. (B) Representative flow cytometry histograms showing CTY signals within L_T in the coculture with CD11b$^+$ cDCs, IMs or AMs in the presence of OVA. (C) Proliferative fraction of L_T in coculture with CD11b$^+$ cDCs, IMs or AMs. (D) Representative flow cytometry histograms showing CTY signals within L_T in the coculture with CD11b$^+$ cDCs, IMs or AMs in the presence (red) or absence (blue) of OVA. (E) Proliferative fraction of L_T in coculture with cDCs, IMs or AMs, with (red) or without (blue) OVA. (F) Representative flow cytometry histograms showing CTY signals within L_T in the coculture with CD11b$^+$ cDCs, IMs or AMs in the presence of MHC-II Ab (blue) or isotype Ab (red). (G) Proliferative fraction of L_T in coculture with cDCs, IMs or AMs in the presence of MHC-II Ab (blue) or isotype Ab (red). (H) Representative flow cytometry histograms showing CTY signals within L_T in the coculture with CD206$^-$MHC-II^{hi} IMs or CD206$^+$MHC-II^{lo} IMs in the presence of OVA. (I) Proliferative fraction of L_T in coculture with CD206$^-$MHC-II^{hi} IMs or CD206$^+$MHC-II^{lo} IMs. (C, E, G, I) Data show mean +/- SD and are pooled from at least 3 independent experiments. Individual values correspond to independent biological replicates. *P* values were calculated with (C) a one-way or (E, G) a two-way analysis of variance (ANOVA) with a Sidak's test for multiple comparisons or (I) a two-tailed unpaired Student's *t* test. **, $P < 0.01$; ***, $P < 0.001$; ns, not significant.

Figure 3. *Ex vivo* induction of Foxp3⁺ Treg by lung IMs is IL-10- and Tgfβ-dependent. (A) Experimental outline. Primary IMs (WT or *Il10*$^{-/-}$), WT CD11b⁺ cDCs or WT AMs were cocultured with OVA-specific naïve L_T for 5 days, and numbers of Foxp3⁺ L_T were evaluated by flow cytometry. (B) Representative flow cytometry plots showing CD4 and intracellular Foxp3 expression within L_T in the coculture with cDCs, IMs or AMs in the presence of OVA. Insets show percentage of Foxp3⁺ cells within CD4⁺ cells. (C) Numbers of Foxp3⁺ L_T in the coculture system shown in (B). (D) UMAP feature plots of the scRNA-seq data analyzed from E-MTAB-7678 (13), as in Figure 1C, according to the expression of *Il10* (left) and *Tgfb1* (right). (E) Representative flow cytometry plots showing CD4 and intracellular Foxp3 expression within L_T in the coculture with IMs and OVA in the presence of Tgfβ Ab or isotype Ab. (F) Numbers of Foxp3⁺ L_T in the coculture system shown in (E). (G) Representative flow cytometry plots showing CD4 and intracellular Foxp3 expression within L_T in the coculture with IMs and OVA in the presence of IL-10 Ab or isotype Ab. (H) Numbers of Foxp3⁺ L_T in the coculture system shown in (G). (I) Representative flow cytometry plots showing CD4 and intracellular Foxp3 expression within L_T in the coculture with WT or *Il10*$^{-/-}$ IMs in the presence of OVA. Insets show percentage of Foxp3⁺ cells within CD4⁺ cells. (J) Numbers of Foxp3⁺ L_T in the coculture system shown in (I). (K) Representative flow cytometry plots showing CD4 and intracellular Foxp3 expression within L_T in the coculture with IMs and OVA in the presence or absence of recombinant Tgfβ (rTgfbβ). (L) Numbers of Foxp3⁺ L_T in the coculture system shown in (K). (C, F, H, J, L) Data show mean +/- SD and are pooled from at least 3 independent experiments. Individual values correspond to independent biological replicates. *P* values were calculated with (C) a one-way analysis of variance (ANOVA) with a Tukey's test for multiple comparisons or (F, H, J, L) a two-tailed unpaired Student's *t* test. **, $P < 0.01$; ***, $P < 0.001$; ****, $P<0.0001$.

Figure 4. IMs can capture OVA *in vivo* and subsequently trigger T cell proliferation and Foxp3$^+$ Tregs *ex vivo*. (A) Representative flow cytometry histograms of FITC signal in lung AMs, IMs, cMo, pMo and cDCs isolated from WT mice exposed intratracheally to 100 µg OVA-FITC and 1 µg LPS or PBS 30 minutes before sacrifice. (B) Quantification of the percentage of FITC$^+$ cells within AMs, IMs, cMo, pMo and cDCs isolated from WT mice exposed intratracheally to PBS or OVA-FITC and LPS 30, 60, 120 and 180 minutes before analysis. (C) Experimental outline for panels (D, E). Primary IMs, cDCs or AMs isolated from WT mice exposed intratracheally to OVA and LPS or PBS 30 minutes before sacrifice were cocultured with CTY-labeled OVA-specific naïve L_T for 3 days, and L_T proliferation was assessed by flow cytometry. (D) Representative flow cytometry histograms showing CTY signals within L_T in the coculture with cDCs, IMs or AMs isolated from WT mice exposed intratracheally to OVA and LPS or PBS 30 minutes before sacrifice. (E) Proliferative fraction of L_T in coculture with cDCs, IMs or AMs, as in (D). (F) Experimental outline for panels (G, H). Primary IMs or AMs isolated from WT mice exposed intratracheally to OVA and LPS 3 hours before sacrifice were cocultured with OVA-specific naïve L_T for 5 days, and numbers of Foxp3$^+$ L_T were evaluated by flow cytometry. (G) Representative flow cytometry plots showing CD4 and intracellular Foxp3 expression within L_T in the coculture with IMs or AMs. Insets show percentage of Foxp3$^+$ cells within CD4$^+$ cells. (H) Numbers of Foxp3$^+$ L_T in the coculture system shown in (G). (B, E, H) Data show mean +/- SD and are pooled from at least 2 (B) or 3 (E, H) independent experiments. Individual values correspond to independent biological replicates. *P* values were calculated with (B, E) a two-way analysis of variance (ANOVA) with a Sidak's test for multiple comparisons or (H) a two-tailed unpaired Student's *t* test. *, $P<0.05$; ****, $P<0.0001$; ns, not significant.

Figure 5. Assessment of IM migratory capacities and IM-CD4$^+$ L$_T$ interactions *in vivo*. (A) Experimental outline for (B, C). (B) Absolute cell numbers of IMs, cDC1 and cDC2 found in the bronchial lymph nodes 20 hours after i.t. injection of 125µg OVA-FITC and 1µg LPS in 50µL or PBS. (C) Absolute cell numbers of FITC$^+$ IMs, cDC1 and cDC2 found in the bronchial lymph nodes 20 hours after i.t. injection of 125µg OVA-FITC and 1µg LPS in 50µL or PBS. (D) Experimental outline for panels (E-G). *Cx3cr1*$^{GFP/+}$ mice were subjected to a mouse model of asthma based on i.t. OVA exposures. (E) Representative images of *Cx3cr1*^{GFP}/MHC-II$^+$ IMs and CD4$^+$ L$_T$ clusters in lungs of mice chronically exposed to OVA. Plain and empty arrowheads indicate *Cx3cr1*^{GFP}/MHC-II$^+$ IMs and CD4$^+$ L$_T$, respectively. (F) Quantification of the distance separating IMs from the closest CD4$^+$ L$_T$ in lungs from control (PBS) or asthmatic (OVA) mice. (G) Numbers of IMs-CD4$^+$ L$_T$ per volume according to the distance separating IMs and CD4$^+$ L$_T$. (B, C, F, G) Data show mean +/- SD, and *P* values were calculated with a (F) Mann-Whitney test or (B, C, G) a two-way analysis of variance (ANOVA) with a Sidak's test for multiple comparisons. ***, $P<0.001$; ****, $P<0.0001$. Lin markers encompassed CD3, CD19, SiglecF, NK1.1 and Ly6G. Scale bars: 20 µm.

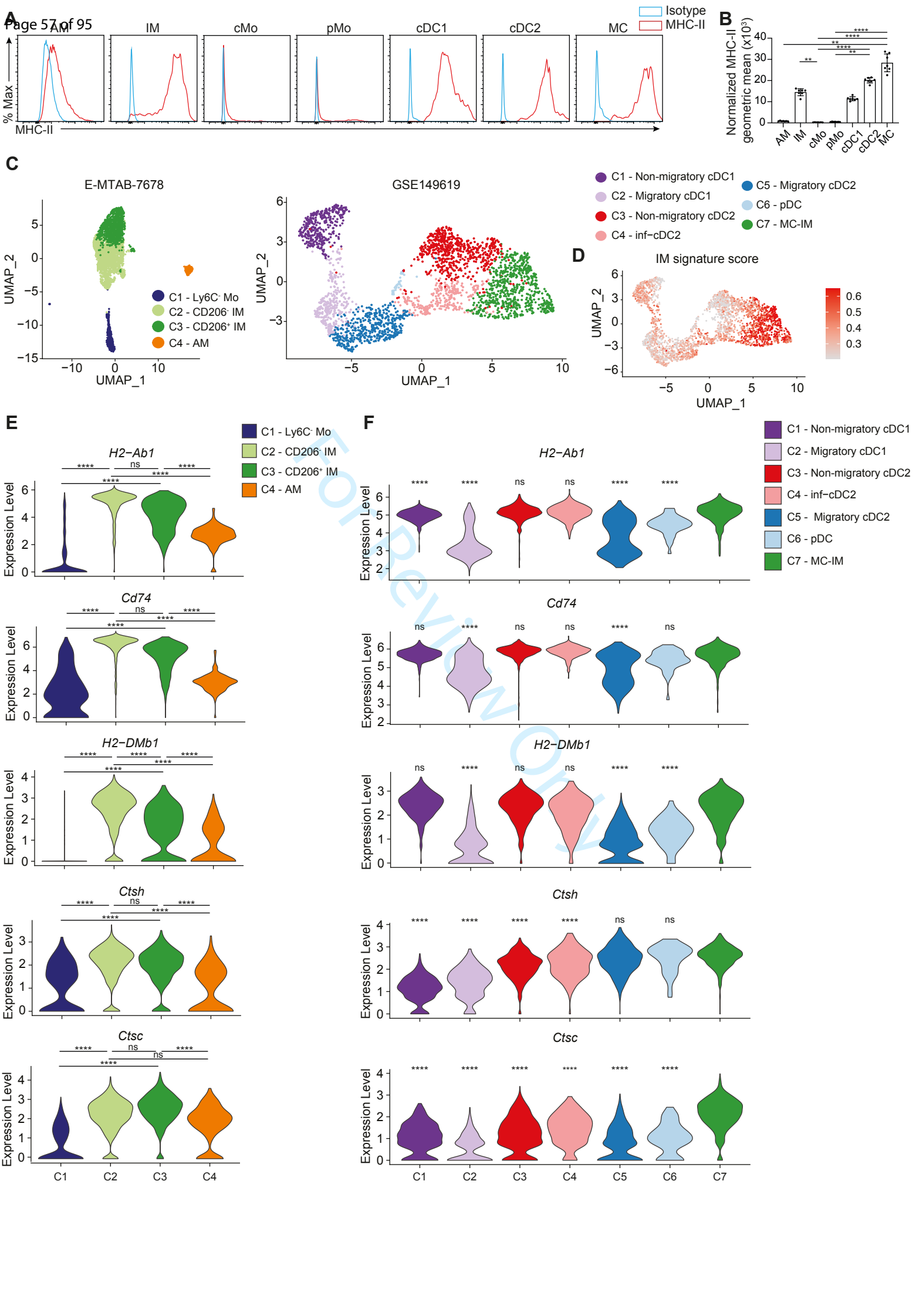

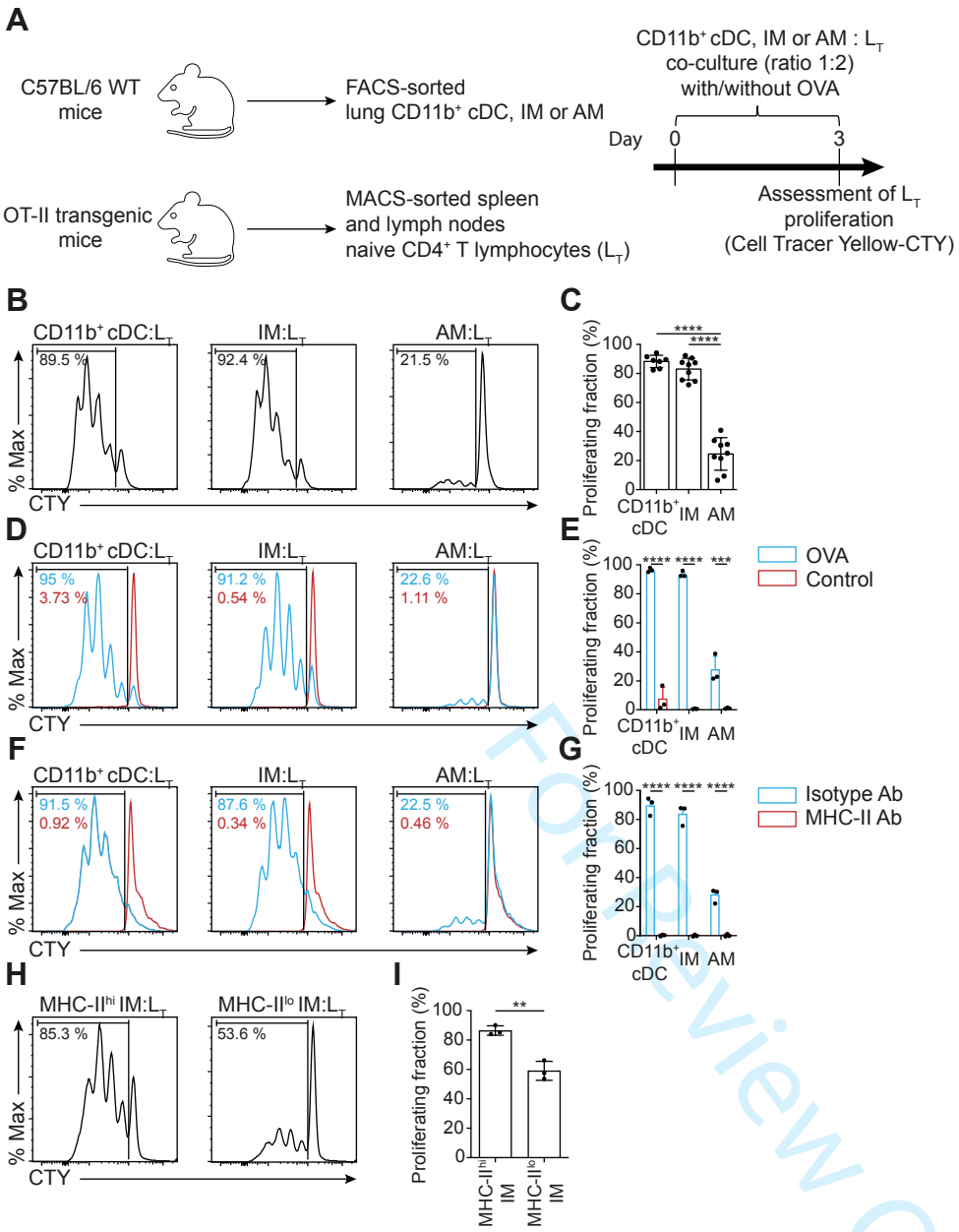

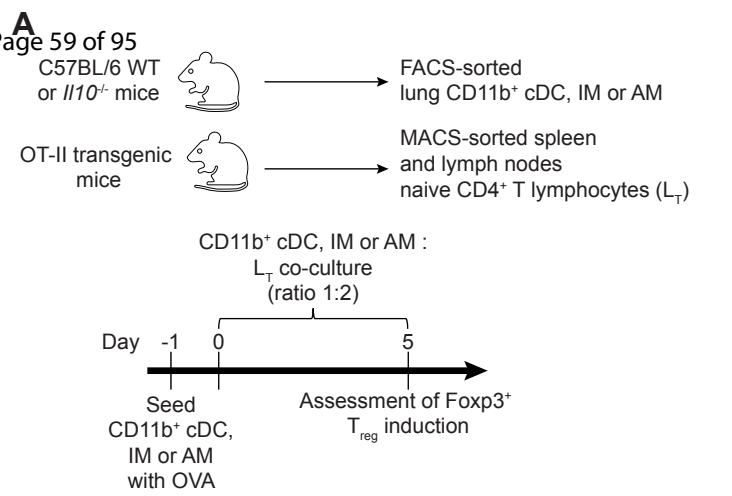

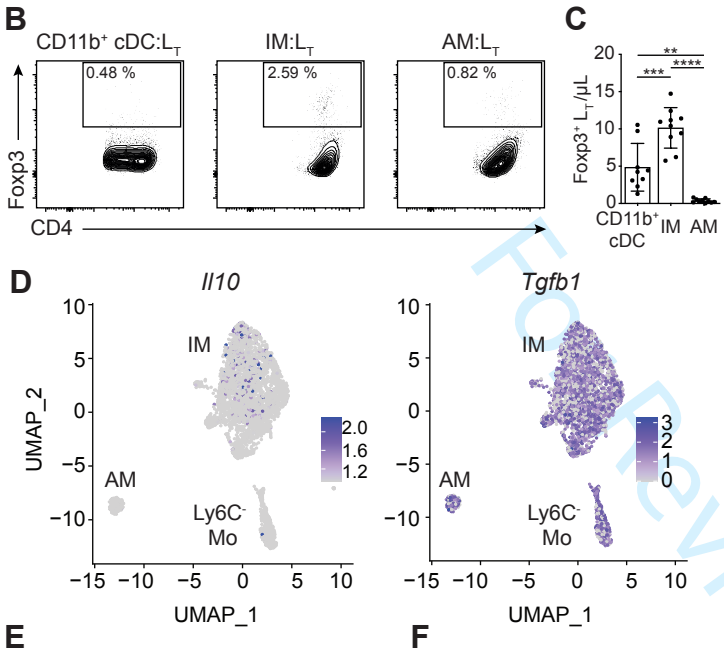

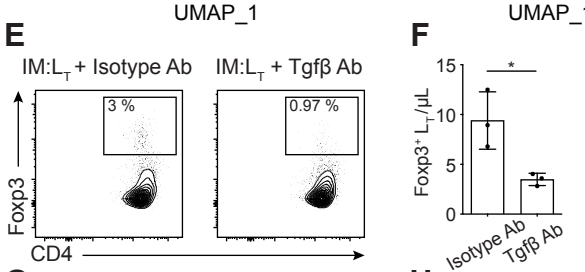

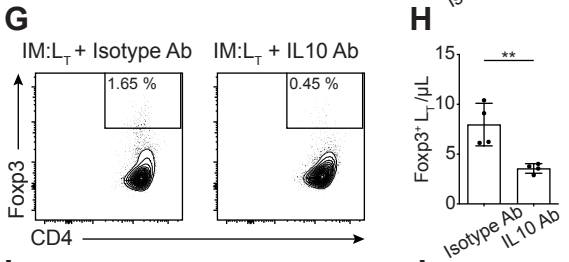

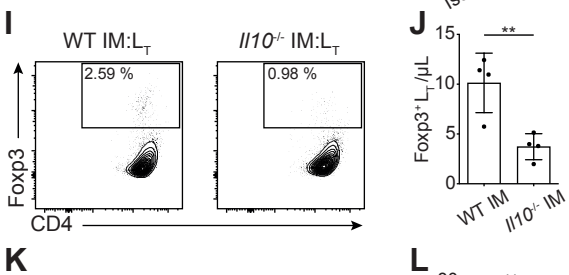

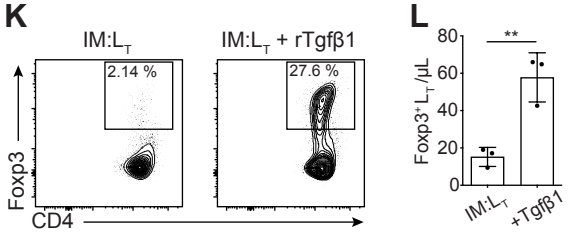

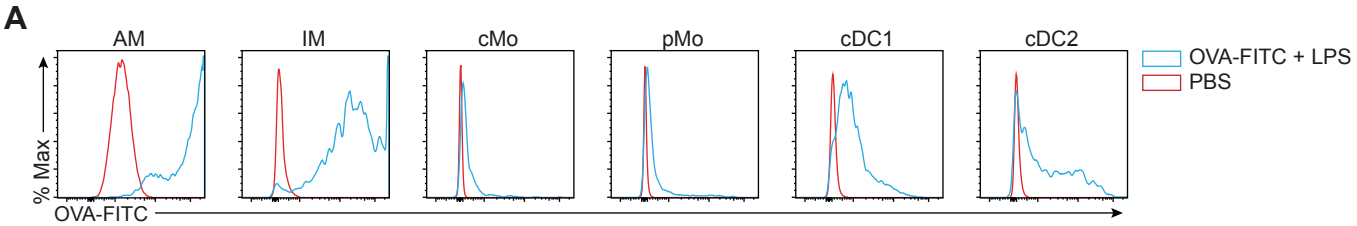

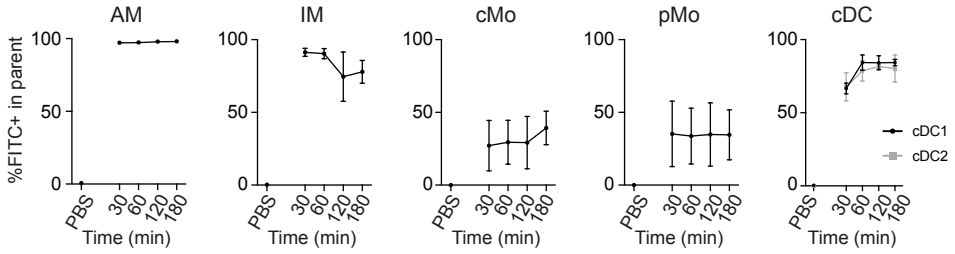

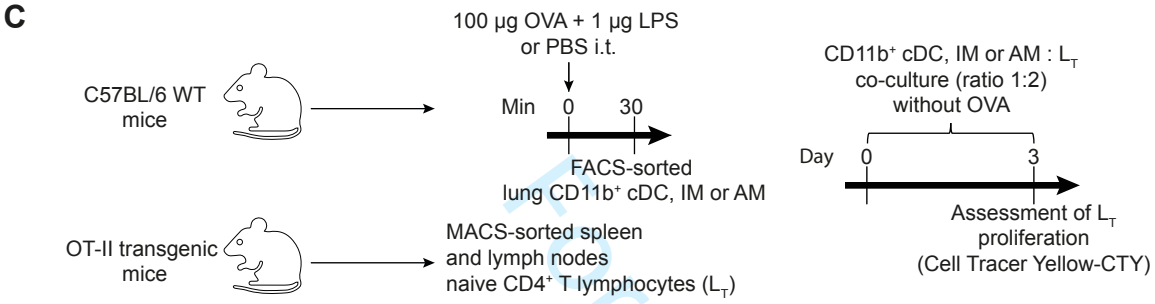

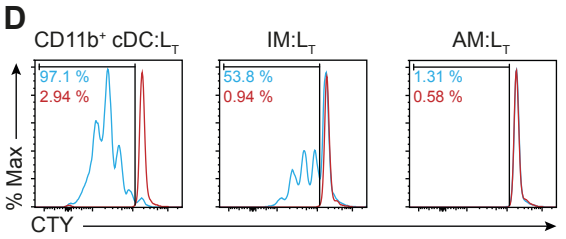

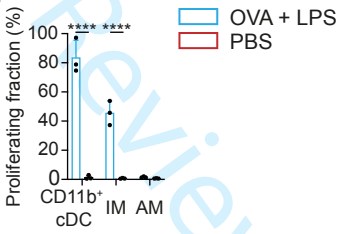

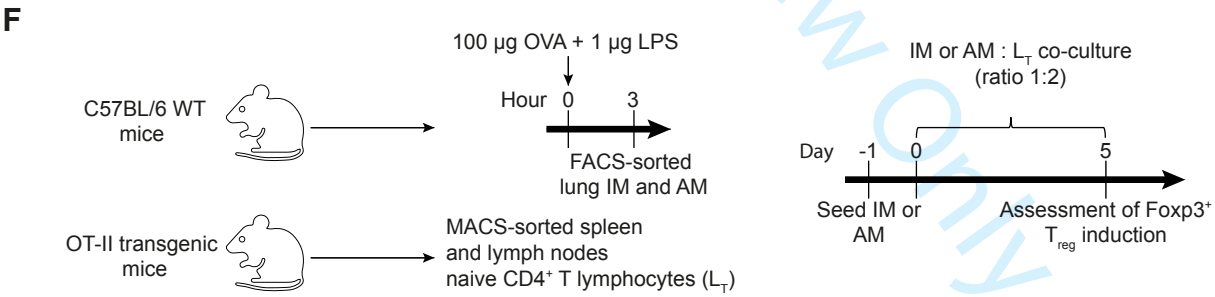

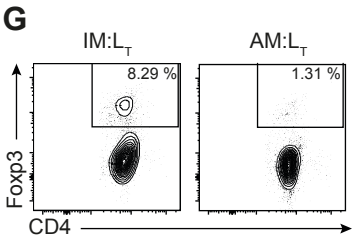

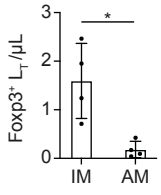

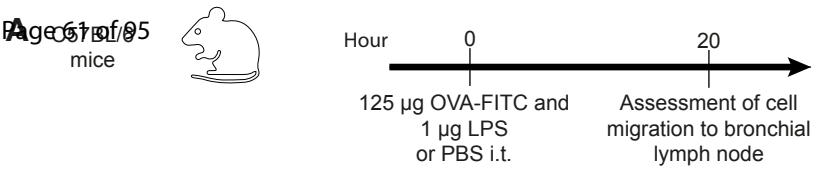

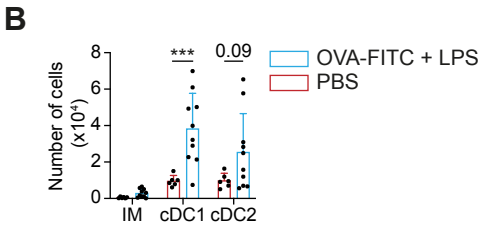

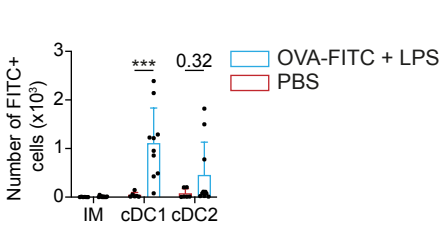

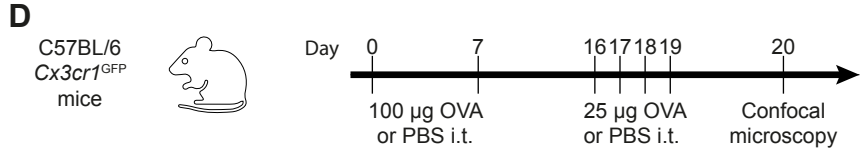

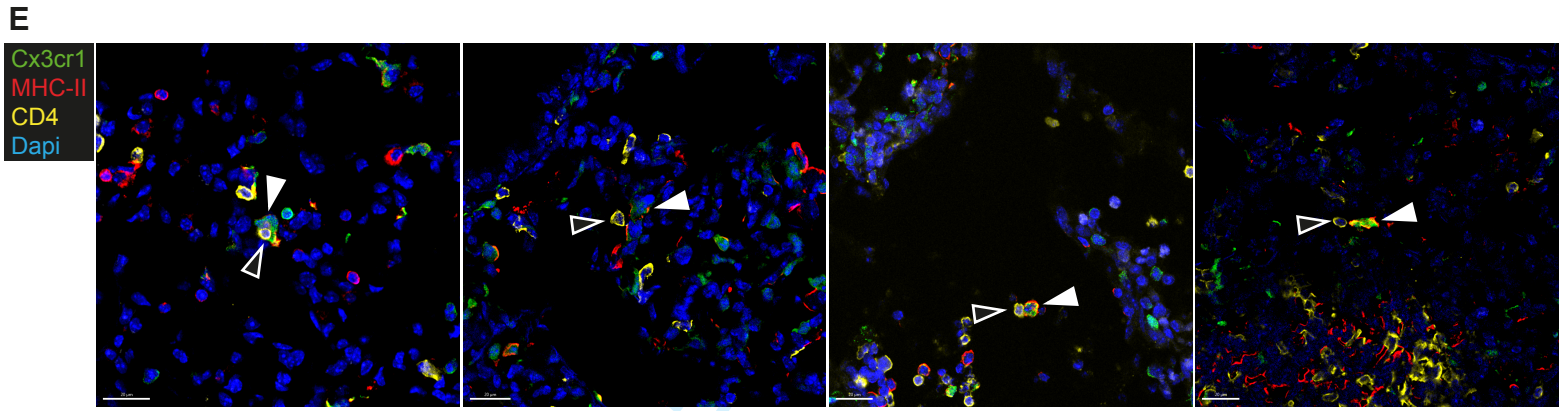

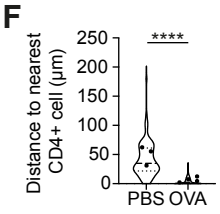

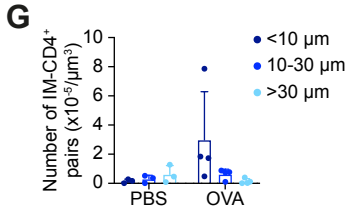

Lung interstitial macrophages can present soluble antigens and induce Foxp3$^+$ regulatory T cells

Authors

Céline Legrand[1], Domien Vanneste[2,3], Alexandre Hego[4], Catherine Sabatel[1,2], Kiréna Mollers[1], Joey Schyns[1,2], Pauline Maréchal[2,3], Joan Abinet[3], Amandine Tytgat[1], Maude Liégeois[1], Barbara Polese[1], Margot Meunier[2,3], Coraline Radermecker[2,3], Laurence Fiévez[1,2], Fabrice Bureau[1,2,*] & Thomas Marichal[2,3,5,*].

Affiliations

[1] Laboratory of Cellular and Molecular Immunology, GIGA Institute, Liège University, Liège, Belgium

[2] Faculty of Veterinary Medicine, Liège University, Liège, Belgium

[3] Laboratory of Immunophysiology, GIGA Institute, Liège University, Liège, Belgium

[4] In Vitro Imaging Platform, GIGA Institute, Liège University, Liège, Belgium.

[5] Walloon Excellence in Life Sciences and Biotechnology (WELBIO) Department, WEL Research Institute, Wavre, Belgium

[*] These authors contributed equally to this work and are co-last authors

Correspondence

Fabrice Bureau
Laboratory of Cellular and Molecular Immunology,
GIGA Institute, Liege University,
Quartier Hôpital, B34,
Avenue de l'Hôpital 11,
4000 Liege, Belgium
f.bureau@uliege.be

Thomas Marichal
Laboratory of Immunophysiology,
GIGA Institute, Liege University,
Quartier Hôpital, B34,
Avenue de l'Hôpital 11,
4000 Liege, Belgium
t.marichal@uliege.be

Supplemental Material and Methods

Mice

All animals and experimental procedures were reviewed and approved by the Institutional Animal Care and Use Committee of the University of Liège (Belgium) (Ethical file #DE1922 & DE2459). The "Guide for the Care and Use of Laboratory Animals", prepared by the Institute of Laboratory Animal Resources, National Research Council, and published by the National Academy Press, as well as European and local legislations, were followed carefully.

Cell Isolation, Staining and Flow cytometry

To obtain single-lung-cell suspensions, lungs were extensively perfused with 10 ml of PBS (Gibco) through the right ventricle, cut into small pieces with razor blades, and digested for 1 h at 37 °C in HBSS containing 5% v/v of FBS (Gibco), 1 mg/ml collagenase A (Sigma) and 0.05 mg/ml DNase I (Roche). After 45 min of digestion, the suspension was flushed using a 18G needle to dissociate aggregates. Cold PBS (Gibco) containing 10mM of EDTA (Merck Millipore) was added to stop the digestion process. The suspension was then filtered and enriched in mononuclear cells by using a density gradient (Percoll from Cytiva) and harvesting cells from the 1.080:1.038 g/ml interface. Lymph nodes were digested in 1mL of the same digestion medium for 15 min at 37°C. They were crushed using a flat-ended syringe and PBS-EDTA was used to stop the digestion process. Staining reactions were performed at 4 °C in FACS buffer (PBS containing 2.5 mg/ml of BSA [Sigma]). Cell phenotyping was performed on a FACSLSRFortessa (BD Biosciences). For cell sorting, cell suspensions were enriched by a magnetic-activated cell sorting (MACS) using anti-mouse CD11b microbeads (Miltenyi Biotec) according to manufacturer's protocol, instead of the density gradient method. The negative fraction was also collected for the staining of AMs. Sorting

was performed on a FACSAriaIII (BD Biosciences) using the nozzle 85. Results were analyzed using FlowJo V10 (Tree Star Inc.).

scRNA-seq analyses

ScRNA-seq data of lung IMs were previously published (1). ScRNA-seq data of lung DCs were previously published(2) and downloaded from an online browser tool provided by the authors (http://bioit2.irc.ugent.be/cdc2/). Filtered matrices containing gene-barcodes and annotation were used to build a Seurat object. Quality control was done by filtering out the cells with less than 200 detected genes, the genes detected in less than three cells and the cells exhibiting more than 5% of mitochondrial genes. Gene counts were normalized by NormalizeData function (Seurat) with a scale factor of 10,000 and log transformation. Two thousands highly variable features were identified with the 'vst' method. Linear dimensional reduction was performed by principle component analysis (PCA) on the scaled data using the RunPCA function (Seurat). The cells were clustered via the FindClusters function (Seurat) with a resolution of 0.5. To visualize the data, non-linear dimensional reduction was used, and UMAP plots were created by using the RunUMAP function (Seurat), with the number of dimensions to use set to first 10 principle components (PCs). Clusters were annotated based on the expression of marker genes described by Bosteels *et al.* (2).

The IM-specific gene signature was calculated using previously published scRNA-seq data(1) by comparing IMs to all other cell types in the dataset using the FindMarker function (Seurat). The genes with |log fold change| > 1 and only positively regulated ones were considered as the IM signature. The signatures were then used to calculate the scores for each cell with the AddModuleScore function (Seurat). The scores were stored in the Seurat object and plotted with Seurat package.

Differentially expressed genes were calculated using the FindAllMarkers function (Seurat).

Confocal microscopy stainings

Lungs from *Cx3cr1*$^{GFP/+}$ mice were perfused with 10ml PBS and infused through the trachea with PAF 4%. Lungs were incubated with PAF 4% for 4 hours at 4°C and then overnight in a 30% sucrose solution. They were embedded and frozen in OCT compound (Q Path Freeze gel, VWR), and cut in 7 µm cryosections and stored at -80°C.

Tissue sections were then fixed in 4% paraformaldehyde for 10 min at room temperature (RT) permeabilized in 0.5% v/v of Triton-X100 (Acros Organics) for 2 min at RT and blocked in PBS containing 12% of BSA (Sigma), 0.5% of Triton-X100, 4% of goat serum (Sigma) and 4% of donkey serum (Sigma) for 1 hour at RT.

Sections were first stained with a rat anti-mouse MHC-II from Invitrogen (dilution 1:500) and rabbit anti-mouse CD4 from Sino Biological (dilution 1:100) overnight at 4 °C. They were then stained with a goat anti-rat AF647 (Invitrogen) (dilution 1:500) and a goat anti-rabbit AF555 (Invitrogen, dilution 1:250) for 1 hour at RT. Third, they were stained with anti-GFP rabbit AF488 from Invitrogen (dilution 1:200) and cell nuclei were counterstained with 4,6- diamidino-2-phenylindole (DAPI, Biolegend) for 1 hour at RT.

Sections were mounted with Prolong Diamond Antifade Mountant (Thermo Fisher) and stored for at least 5 hours at RT. Samples were rinsed 3 times in PBS between each of the above-mentioned steps and stainings were done in a solution containing PBS-BSA 1%, Triton-X100 0.4%, goat and donkey serum 3,5% each.

Confocal microscopy acquisition and analysis

The images were acquired using a Leica Stellaris 8 inverted confocal microscope in confocal mode, equipped with a Plan-Apochromat 40x/1.3 oil objective. The imaging parameters were set as follows: DAPI was imaged using a 405 nm laser at 10.8% power, AOBS (Acousto-Optical Beam Splitter) set at 425 nm - 487 nm, and gains at 52; CX3CR1 AF488 was imaged using a 499 nm laser at 2.7% power, AOBS set at 504 nm - 556 nm, and gains at 34.2; CD4 AF555 was imaged using a 553 nm laser at 2.94% power, AOBS set at 565 nm - 635 nm; and MHCII AF647 was imaged using a 653 nm laser at 2.87% power, AOBS set at 658 nm - 834 nm, and gains at 3.7. Each tile was acquired with 512 x 512 pixels, corresponding to 184.52 µm x 184.52 µm, at a speed of 400 Hz. We performed 3D, with images every 1 µm, and large image scanning of lung sections to cover a larger tissue volume. The acquired images were stitched together and saved in the .lif format.

Upon importing the acquired images into Imaris 9.5, we performed cell segmentation using the available surface and spot tools within the software. By leveraging the specific markers expressed by the two types of immune cells, we successfully identified and classified them accordingly. Subsequently, we utilized the distance measurement function within Imaris to calculate the minimum intercellular distance between cells of different types. This advanced feature allowed us to obtain precise measurements of the intercellular distance in micrometers (µm) for each cell pair. All Imaris analyses were performed in batch mode, using the same algorithm to detect cells in all images.

Supplemental References

1. Schyns J, Bai Q, Ruscitti C, Radermecker C, De Schepper S, Chakarov S, *et al.* Non-classical tissue monocytes and two functionally distinct populations of interstitial macrophages populate the mouse lung. *Nat Commun* 2019;10:3964.
2. Bosteels C, Neyt K, Vanheerswynghels M, van Helden MJ, Sichien D, Debeuf N, *et al.* Inflammatory Type 2 cDCs Acquire Features of cDC1s and Macrophages to Orchestrate Immunity to Respiratory Virus Infection. *Immunity* 2020;52:1039-1056.e9.

Supplemental Tables

Table E1. List of antibodies and reagents used in flow cytometry, confocal microscopy and culture experiments.

Antibodies and staining reagents for flow cytometry		
PE-Cy7 rat anti-CD11b, clone M1/70	BD Pharmingen	561098
APC-Cy7 Hamster anti-mouse CD11c, clone HL3	BD Pharmingen	561241
BUV395 Hamster anti-mouse CD11c, cloneHL3	BD Horizon	564080
APC anti-mouse CD172a, clone P84	Biolegend	144013
PE rat anti-mouse CD19, clone 1D3	BD Pharmingen	553786
BV786 rat anti-mouse CD26, clone H194-112	BD Optibuild	740868
PE Hamster anti-mouse CD3, clone 145-2C11	BD Pharmingen	553064
PerCP-Cy5.5 rat anti-mouse CD4, clone RM4-5	BD Pharmingen	550954
V500 Mouse anti-mouse CD45.2, clone 104	BD Horizon	562130
BV421 anti-mouse CD64, clone X54-5/7.1	Biolegend	139309
CellTrace Yellow Cell proliferation kit	Invitrogen	C34573
BV605 anti-mouse F4/80, clone BM8	Biolegend	123133
PE anti-mouse F4/80, clone BM8	eBioscience	12-4801-82
PE rat anti-Foxp3, clone FJK-16s	eBioscience	12-5773-82
APC rat anti-mouse Ly6C, clone AL21	BD Pharmingen	560595
FITC rat anti-mouse Ly6C, clone AL21	BD Pharmingen	553104
PE-CF594 Rat anti-mouse Ly6C, clone AL21	BD Horizon	562728
PE Rat anti-Mouse Ly6G, clone 1A8	BD Pharmingen	551461
PE-Cy7 anti-mouse FceRIa, clone MAR-1	Biolegend	134317
APC Mouse anti-mouse I-A(b), clone AF6-120.1	BD Pharmingen	562823
FITC anti-mouse I-A(b), clone AF6-120.1	BD Pharmingen	562011
PerCP-Cy5.5 anti-mouse I-A/I-E, clone M5/114.15.2	Biolegend	107626
PE Mouse anti-mouse NK1.1, clone PK136	BD Pharmingen	553165
PE rat anti-mouse Siglec-F, clone E50-2440	BD Pharmingen	552126
Fixable viability dye ef660	eBioscience	65-0864-14
APC-Cy7 anti mouse/rat XCR1, clone ZET	Biolegend	148223
Antibodies for confocal microscopy		
rat anti-mouse MHC-II	Invitrogen	14-5321-85
rabbit anti-mouse CD4	Sino biological	50134-R711
Goat anti rabbit IgG AF555	invitrogen	A21429
Goat anti rat IgG AF647	invitrogen	A21247
anti-GFP rabbit AF488	invitrogen	A21311

Antibodies for culture experiments		
purified monoclonal igG anti-TGF-B(1,2,3), clone 1D1	RandD systems	MAB 1835
anti-mouse cd3e purified, clone 145-2C11	ebioscience	14-0031-85
anti-mouse CD28 purified, clone 37.51	eBioscience	14-0281-85
Purified NA/LE rat anti-mouse IL-10	BD Bioscience	554463
LEAF purified anti-mouse I-A / I-E, clone M5/114.15.2	Biolegend	107610
Isotype control antibodies		
IgG2a-FITC, isotype control	Sigma	F6522
IgG1 isotype control, clone 11711	RandD systems	MAB002
Purified NA:LE Rat IgG2b,k isotype control	BDbioscience	556968
LEAF Purified Rat IgG2b,k isotype cntrol, clone RTK4530	Biolegend	400622

138

Supplemental Figures and Legends

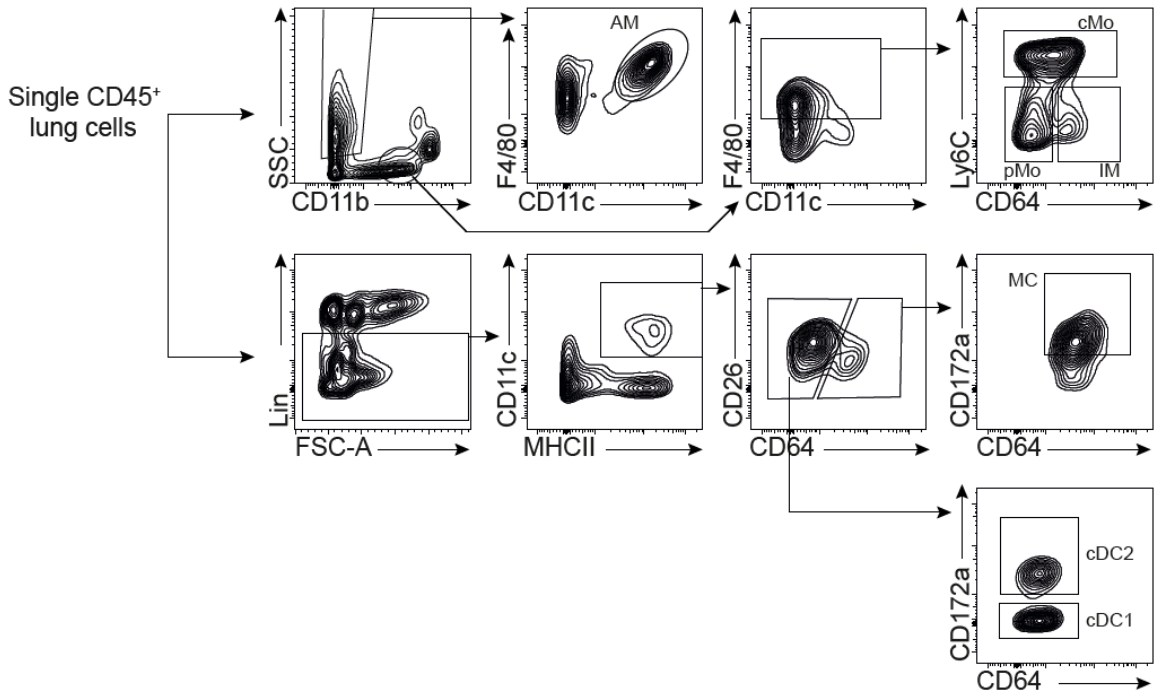

Figure E1. Flow cytometry gating strategies to delineate lung monocytes, macrophages and DCs. Flow cytometry gating strategies to delineate $CD45^+SSC^{hi}F4/80^+CD11c^+$ AMs, $CD45^+SSC^{lo}CD11b^+F4/80^+Ly6C^-CD64^+$ IMs, $CD45^+SSC^{lo}CD11b^+F4/80^+Ly6C^+CD64^-$ classical monocytes (cMo), $CD45^+SSC^{lo}CD11b^+F4/80^+Ly6C^-CD64^-$ patrolling monocytes (pMo), $CD45^+Lin^-CD11c^+MHC\text{-}II^+CD64^-CD26^+CD172a^-$ cDC1s, $CD45^+Lin^-CD11c^+MHC\text{-}II^+CD64^-CD26^+CD172a^+$ cDC2s and monocyte-derived CD64+ cells (MCs), defined as $CD45^+Lin^-CD11c^+MHC\text{-}II^+CD64^+CD26^-CD172a^+$ cells.

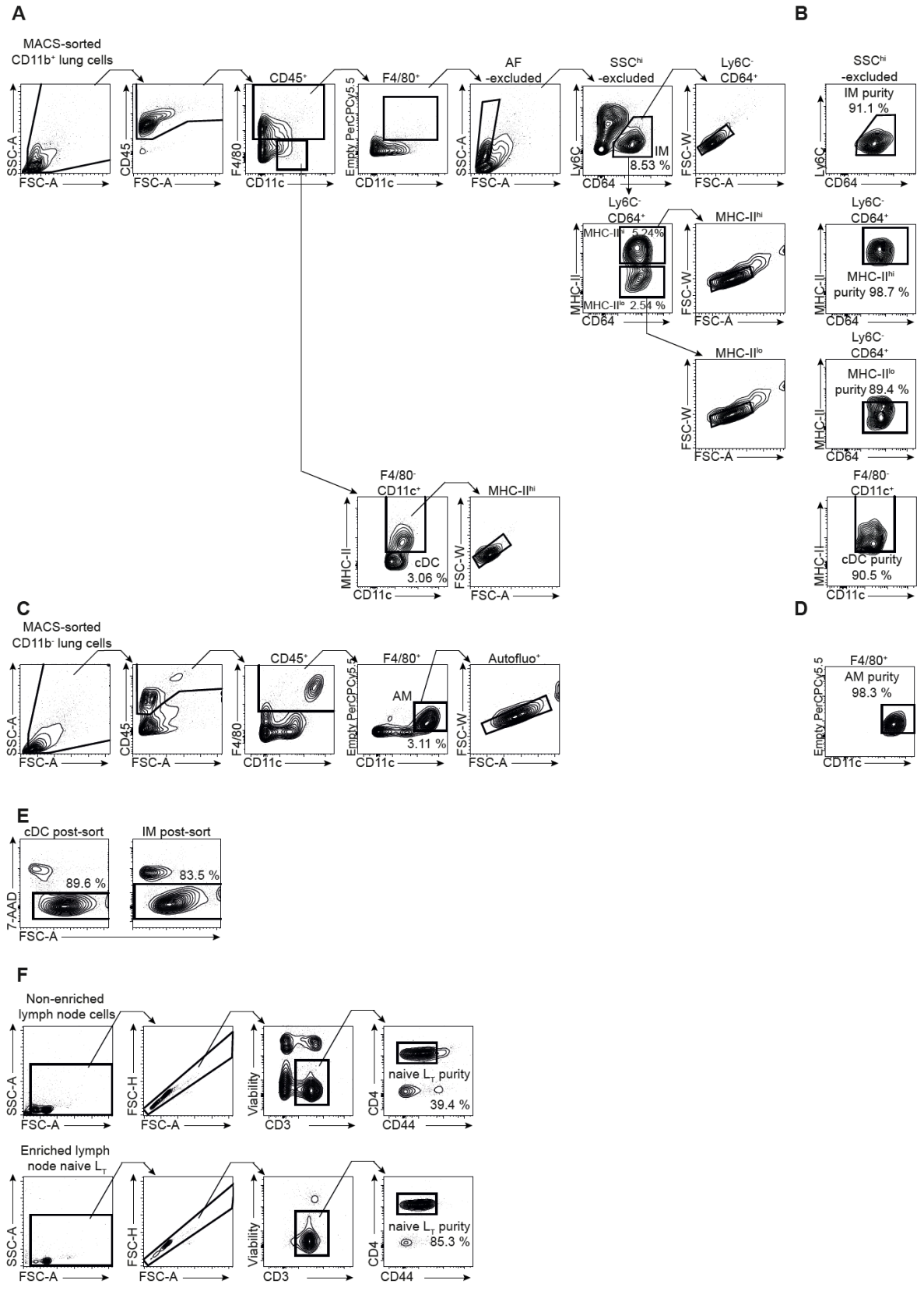
A
MACS-sorted CD11b+ lung cells
SSC-A
FSC-A
CD45
CD45+
F4/80
CD11c
F4/80+
Empty PerCPCy5.5
AF -excluded
SSChi -excluded
Ly6C
CD64
IM 8.53 %
Ly6C- CD64+
FSC-W
MHC-II
MHC-IIhi 5.24%
MHC-IIlo 2.54 %
MHC-IIhi
MHC-IIlo
F4/80- CD11c+
cDC 3.06 %
B
SSChi -excluded
IM purity 91.1 %
Ly6C- CD64+
MHC-IIhi purity 98.7 %
MHC-IIlo
MHC-IIlo purity 89.4 %
F4/80- CD11c+
cDC purity 90.5 %
C
MACS-sorted CD11b- lung cells
Autofluo+
AM
3.11 %
D
F4/80+
AM purity 98.3 %
E
cDC post-sort
IM post-sort
89.6 %
83.5 %
7-AAD
F
Non-enriched lymph node cells
FSC-H
Viability
CD3
CD4
CD44
naive LT purity 39.4 %
Enriched lymph node naive LT
naive LT purity 85.3 %

148

149

Figure E2. Flow cytometry sorting strategy to isolate lung IMs, MHC-II^{high} IMs, MHC-II^{low} IMs, CD11b^{+} cDCs and AMs, and assessment of post-sort purity and viability. (A) Representative FACS sorting strategy of IMs, MHC-II^{high} IMs, MHC-II^{low} IMs and CD11b^{+} cDCs after MACS CD11b^{+} cell enrichment of lung single-cell suspensions. (B) Post-sort purity of FACS-sorted IMs, MHC-II^{high} IMs, MHC-II^{low} IMs and CD11b^{+} cDCs. Representative post-sort flow cytometry dot plots are shown. (C) Representative FACS sorting strategy of AMs isolated from the negative fraction of the MACS CD11b^{+} cell enrichment (CD11b^{-}) of lung single-cell suspensions. (D) Post-sort purity of FACS-sorted AMs. Representative post-sort flow cytometry dot plots are shown. (E) Post-sort viability of CD11b^{+} cDCs and IMs. Representative 7-AAD and FSC dot plots are shown. (F) Representative flow cytometry gating strategy to delineate naïve L_T in lymph node single-cell suspensions, before (top) and after (bottom) MACS enrichment. (A, C, F) Insets indicate the percentage of cells within the total cells. (B, D, E) Insets indicate the percentage of cells within the indicated gate.

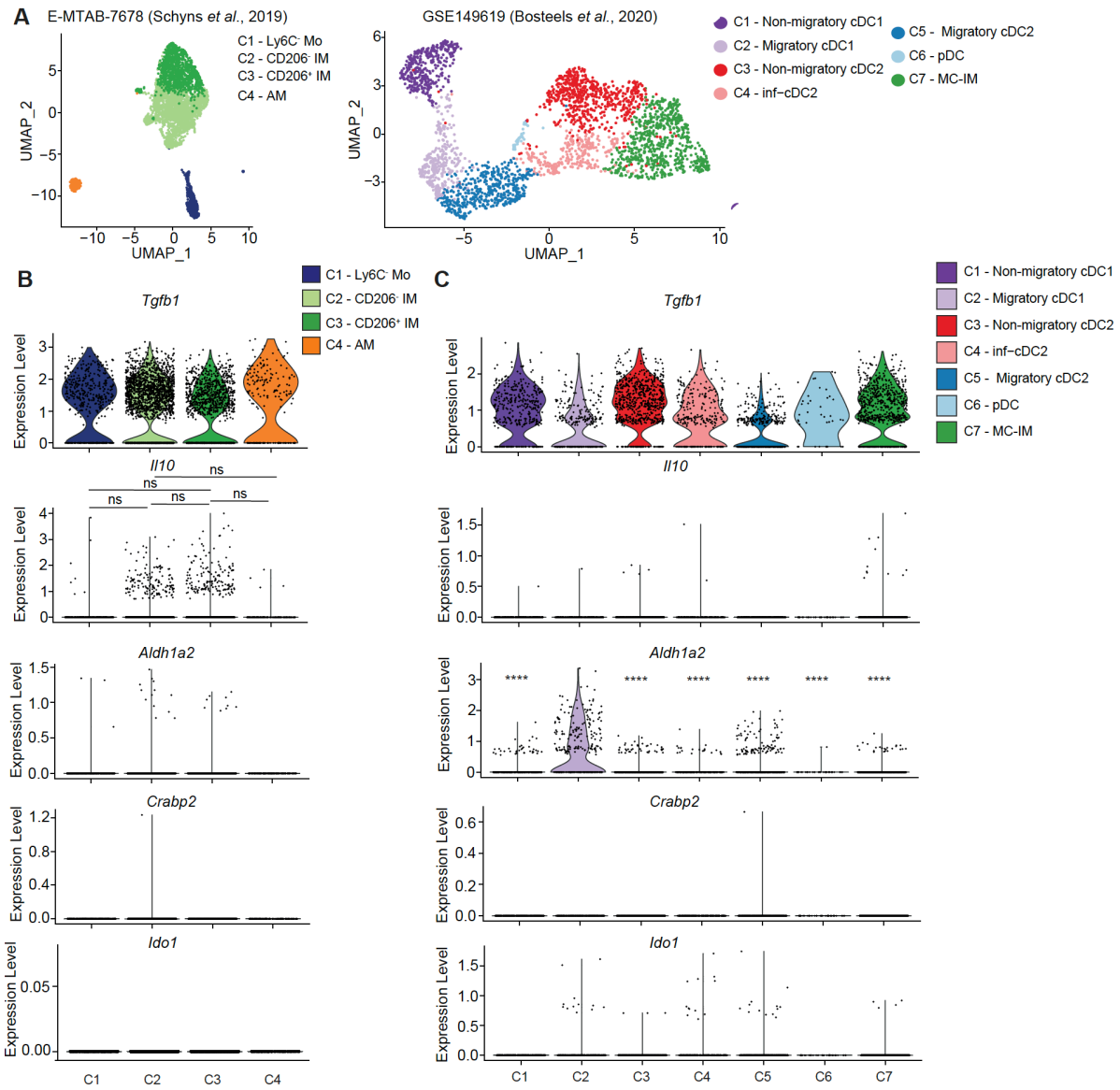

Figure E3. Expression of genes associated with T_{reg} induction in lung myeloid cells. (A) UMAP plots of the scRNA-seq data analyzed from E-MTAB-7678 (13) (left) and from GSE149619 (9) (right). (B) Expression of the indicated genes in lung CD16.2$^+$ monocytes, CD206$^+$ IMs, CD206$^-$ IMs and AMs, as depicted by violin plots (height: expression level; width: abundance of cells). (C) Expression of the indicated genes in lung cDC subsets, plasmacytoid DCs (pDCs) and MC-IMs, as depicted by violin plots (height: expression level; width: abundance of cells). To compare C2 – CD206$^-$IMs, C3 – CD206$^+$ IMs in (B) and C7 – Migratory cDC1s in (C) with other groups, *P* values were calculated using a Wilcoxon rank sum test. ****, *P*<0.0001; ns, not significant.

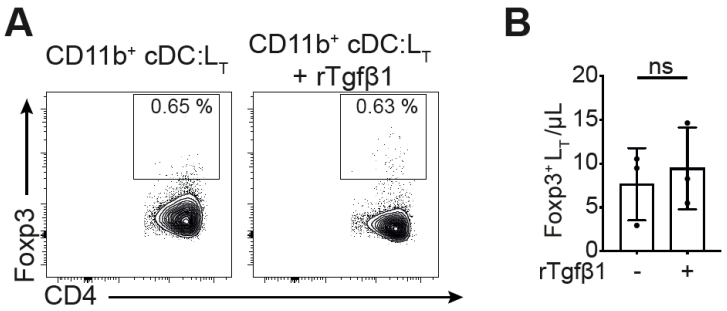

Figure E4. Addition of recombinant Tgfβ does not boost the ability of cDCs to induced Foxp3⁺ L_T. (A) Representative flow cytometry plots showing CD4 and intracellular Foxp3 expression within OVA-specific L_T 5 days after co-culture with cDCs and OVA in the absence or presence of recombinant Tgfβ. (B) Numbers of Foxp3⁺ L_T in the co-culture system shown in (A). Data show mean +/- SD and are pooled from 3 independent experiments. Individual values correspond to independent biological replicates. *P* values were calculated with a two-tailed unpaired Student's *t* test.

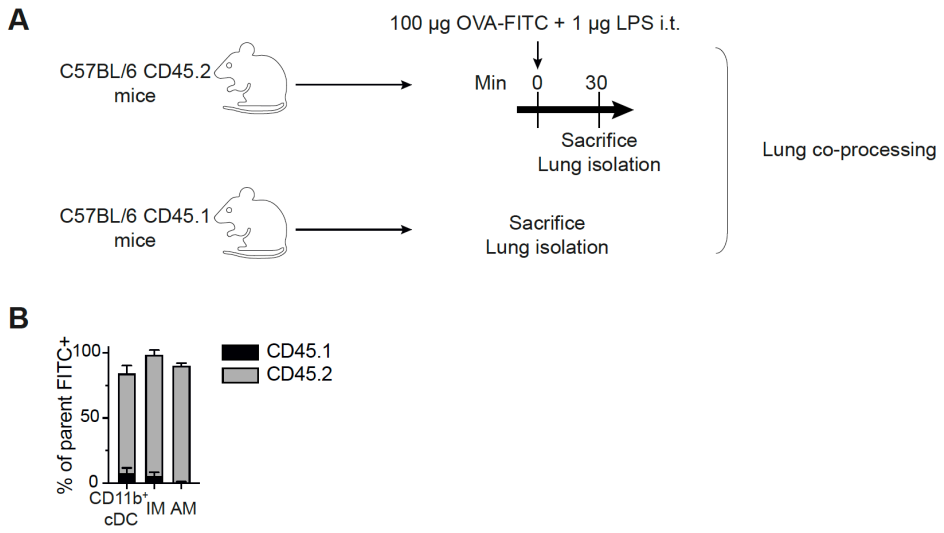

Figure E5. After *in vivo* OVA-FITC exposure, uptake by cDCs, AMs and IMs occurs *in vivo* and not during the tissue processing *ex vivo*. (A) Experimental outline. Lung pieces of CD45.2$^+$ WT mice exposed to 100 µg OVA-FITC and 1 µg LPS i.t. 30 minutes before sacrifice were mixed with lung pieces of naïve CD45.1$^+$ WT mice and the lungs were co-digested and co-processed together. The percentage of CD45.2$^+$ or CD45.1$^+$ FITC$^+$ cDCs, IMs and AMs was then assessed by flow cytometry. (B) Quantification of the percentage of FITC$^+$ cDCs, IMs and AMs of CD45.2 or CD45.1 origin. Data show mean +/- SD and are pooled from 2 independent experiments. Individual values correspond to independent biological replicates.

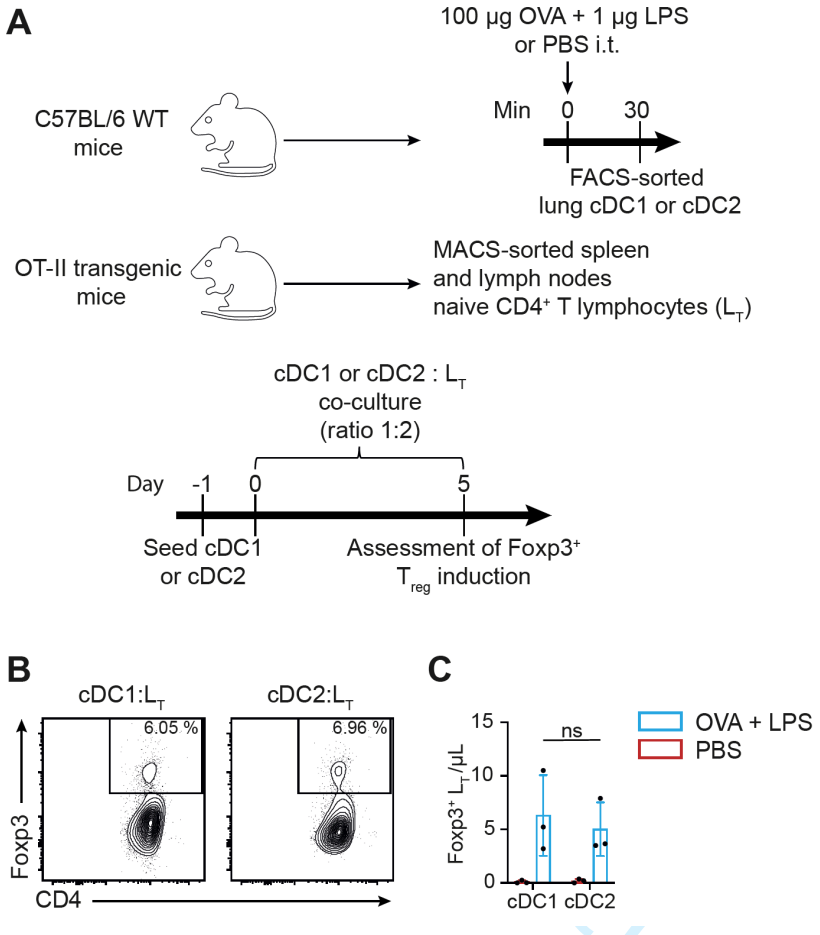

Figure E6. Ability of cDC1s and cDC2s sorted from OVA-pulsed WT mice to induce T_{reg} *ex vivo*. (A) Experimental outline for panels (B, C). Primary cDC1s or cDC2s isolated from WT mice exposed intratracheally to OVA and LPS 30 minutes before sacrifice were cocultured with OVA-specific naïve L_T for 5 days, and numbers of Foxp3$^+$ L_T were evaluated by flow cytometry. (B) Representative flow cytometry plots showing CD4 and intracellular Foxp3 expression within L_T in the coculture with cDC1s or cDC2s. Insets show percentage of Foxp3$^+$ cells within CD4$^+$ cells. (C) Numbers of Foxp3$^+$ L_T in the coculture system shown in (B). Data show mean +/- SD and are pooled from at 3 independent experiments. Individual values correspond to independent biological replicates. *P* values were calculated with a two-way analysis of variance (ANOVA) with a Sidak's test for multiple comparisons. ns, not significant.

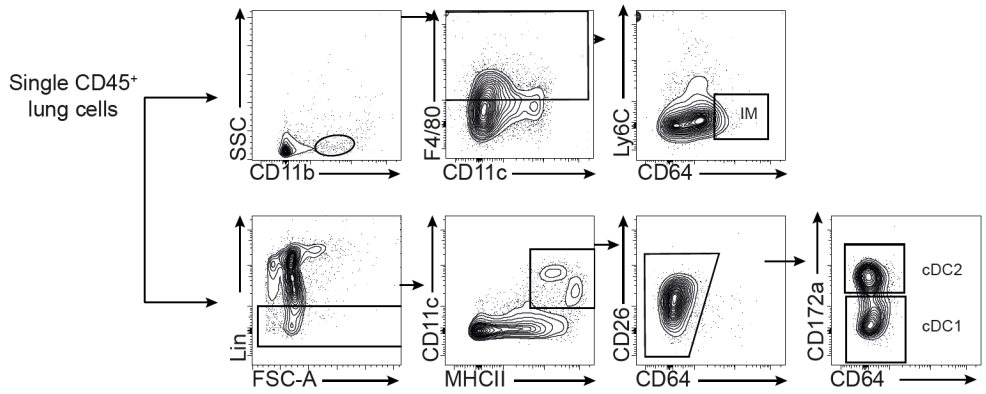

Figure E7. Flow cytometry gating strategies to delineate lymph node IMs, cDC1s and cDC2s. Flow cytometry gating strategies to delineate $CD45^+SSC^{lo}CD11b^+F4/80^+Ly6C^-CD64^+$ IMs, $CD45^+Lin^-CD11c^+MHC\text{-}II^+CD64^-CD26^+CD172a^-$ cDC1s and $CD45^+Lin^-CD11c^+MHC\text{-}II^+CD64^-CD26^+CD172a^+$ cDC2s in the lymph nodes.